

OBSERVATIONAL CONSTRAINTS ON THE TILTED FLAT- Λ CDM AND THE UNTILTED NONFLAT Λ CDM DYNAMICAL DARK ENERGY INFLATION PARAMETERIZATIONS

CHAN-GYUNG PARK^{1,2} AND BHARAT RATRA²

(Dated: July 29, 2019)
Draft version July 29, 2019

ABSTRACT

We constrain tilted spatially-flat and untilted nonflat Λ CDM dynamical dark energy inflation parameterizations using Planck 2015 cosmic microwave background (CMB) anisotropy data and recent baryonic acoustic oscillations distance measurements, Type Ia supernovae data, Hubble parameter observations, and growth rate measurements. Inclusion of the four non-CMB data sets results in a significant strengthening of the evidence for nonflatness in the nonflat Λ CDM model from 1.1σ for the CMB data alone to 3.4σ for the full data combination. In this untilted nonflat Λ CDM case the data favor a spatially-closed model in which spatial curvature contributes a little less than a percent of the current cosmological energy budget; they also mildly favor dynamical dark energy over a cosmological constant at 1.2σ . These data are also better fit by the flat- Λ CDM parameterization than by the standard Λ CDM model, but only at 0.3σ significance. Current data is unable to rule out dark energy dynamics. The nonflat Λ CDM parameterization is compatible with the Dark Energy Survey limits on the present value of the rms mass fluctuations amplitude (σ_8) as a function of the present value of the nonrelativistic matter density parameter (Ω_m), however it does not provide as good a fit to the higher multipole CMB temperature anisotropy data as does the standard tilted flat- Λ CDM model. A number of measured cosmological parameter values differ significantly when determined using the tilted flat- Λ CDM and the nonflat Λ CDM parameterizations, including the baryonic matter density parameter and the reionization optical depth.

Subject headings: cosmological parameters — cosmic background radiation — large-scale structure of universe — inflation — observations — methods:statistical

1. INTRODUCTION

In the standard spatially-flat Λ CDM cosmological model (Peebles 1984) the current cosmological energy budget is dominated by the cosmological constant Λ which powers the currently accelerating cosmological expansion. Cold dark matter (CDM) and baryonic matter are the next two largest contributors to the current energy budget, followed by small contributions from neutrinos and photons. For reviews of the standard model see Ratra & Vogeley (2008), Martin (2012), Brax (2018), and Luković et al. (2018). This model is able to accommodate most observational constraints, including CMB anisotropy measurements (Planck Collaboration 2016), baryonic acoustic oscillation (BAO) distance observations (Alam et al. 2017), Hubble parameter data (Farooq et al. 2017),³ and Type Ia supernova (SNIa) apparent magnitude measurements (Scolnic et al. 2017). Current observational constraints however allow for slightly nonflat spatial geometries and/or mild dark energy dynamics.

The standard spatially-flat Λ CDM inflation model is characterized by six cosmological parameters conventionally chosen to be: $\Omega_b h^2$ and $\Omega_c h^2$, the current values of the baryonic and cold dark matter density parameters multiplied by

the square of the Hubble constant H_0 (in units of $100 \text{ km s}^{-1} \text{ Mpc}^{-1}$); τ , the reionization optical depth; θ_{MC} , the angular diameter distance as a multiple of the sound horizon at recombination; and n_s and A_s , the spectral index and amplitude of the power-law primordial scalar fractional energy density spatial inhomogeneity power spectrum.

Observational data are on the verge of being able to place interesting constraints on seven parameter cosmological models. Two more plausible seventh cosmological parameters now under discussion are spatial curvature in nonflat extensions of the standard model and a parameter that governs dark energy dynamics in dynamical dark energy extensions of the standard model.

A simple, and so widely used, dynamical dark energy parameterization is the XCDM one.⁴ This parameterizes the equation of state relation between the pressure and energy density of the dark energy fluid through $p_X = w\rho_X$ where the equation of state parameter w is the additional seventh cosmological parameter. XCDM is not a physically consistent description of dark energy as it is unable to consistently describe the evolution of energy density spatial inhomogeneities. To render XCDM physically consistent requires an eighth cosmological parameter, the square of the speed of sound in the dark energy fluid, $c_{sX}^2 = dp_X/d\rho_X$. In this paper, as is common practice, we consider a restricted, physically-consistent, modified XCDM parameterization in which c_{sX}^2 is not allowed to vary in space or with time and is arbitrarily set to unity. ϕ CDM is the simplest physically consistent dynamical dark energy model (Peebles & Ratra 1988; Ratra & Peebles 1988). Here a scalar field ϕ with potential energy density $V(\phi) \propto \phi^{-\alpha}$

¹ Division of Science Education and Institute of Fusion Science, Chonbuk National University, Jeonju 54896, South Korea; e-mail: park.chan.gyung@gmail.com

² Department of Physics, Kansas State University, 116 Cardwell Hall, Manhattan, KS 66506, USA

³ Hubble parameter values have been measured from low redshift to well past the redshift of the cosmological deceleration-acceleration transition between the earlier nonrelativistic-matter-dominated decelerating cosmological expansion and the more recent dark-energy-dominated accelerating cosmological expansion. The transition redshift has been measured from Hubble parameter observations and it is roughly at the value expected in dark energy models (Farooq & Ratra 2013; Moresco et al. 2016; Farooq et al. 2017; Yu et al. 2018).

⁴ Many observations have been used to constrain the XCDM parameterization (see, e.g., Chen & Ratra 2004; Samushia et al. 2007; Samushia & Ratra 2010; Chen & Ratra 2011b; Solà et al. 2017a, 2018, 2017b,c,d; Zhai et al. 2017, and references therein).

is the dynamical dark energy with $\alpha > 0$ being the additional seventh cosmological parameter.⁵

Ooba et al. (2018d) (also see Park & Ratra 2018b) have analyzed the Planck 2015 CMB anisotropy data and some BAO distance measurements by using these seven parameter tilted spatially-flat XCDM and ϕ CDM dynamical dark energy inflation models and found that both were slightly favored by the data, compared to the standard six parameter flat- Λ CDM model, by 1.1σ (1.3σ) for the XCDM (ϕ CDM) case. While these are not significant improvements over the standard model, current data are not able to rule out dark energy dynamics. In addition, both dynamical dark energy models reduce the tension between the Planck 2015 CMB anisotropy and the weak gravitational lensing constraints on σ_8 , the rms fractional energy density spatial inhomogeneity averaged over $8h^{-1}$ Mpc radius spheres.

There have been a number of earlier suggestions that different combinations of observational data favor dynamical dark energy models over the standard Λ CDM model (Sahni et al. 2014; Ding et al. 2015; Solà et al. 2015; Zheng et al. 2016; Solà et al. 2017a, 2018, 2017b; Zhao et al. 2017; Solà et al. 2017c; Zhang et al. 2017a; Solà et al. 2017d; Gómez-Valent & Solà 2017; Cao et al. 2018; Gómez-Valent & Solà 2018). As far as we are aware, of these analyses, only those of Zhao et al. (2017) and Zhang et al. (2017a) performed complete CMB anisotropy analyses of the generalized XCDM dynamical dark energy parameterizations they assumed.⁶ The other analyses either ignored CMB anisotropy data or only approximately accounted for it.

The standard Λ CDM model assumes flat spatial hypersurfaces. In nonflat models non-vanishing spatial curvature introduces a new length scale and so it is incorrect to assume a power spectrum for energy density inhomogeneities in nonflat models that does not correctly account for the spatial curvature length scale (as was assumed for analyses of nonflat models in Planck Collaboration 2016). Nonflat cosmological inflation provides the only known method for computing a physically consistent power spectrum in nonflat models. For open spatial hypersurfaces the Gott (1982) open-bubble inflation model is used to compute the non-power-law power spectrum (Ratra & Peebles 1994, 1995). For closed spatial hypersurfaces Hawking’s prescription for the initial quantum state of the universe (Hawking 1984; Ratra 1985) is used to define a closed inflation model that gives the non-power-law power spectrum of spatial inhomogeneities (Ratra 2017). In the nonflat inflation models, compared to the flat inflation model, there is no simple way to allow for tilt so n_s is not a free parameter and it is replaced by the present value of the spatial curvature density parameter Ω_k .

Using such a physically consistent untilted nonflat inflation model non-power-law power spectrum of energy density inhomogeneities, Ooba et al. (2018a) found that Planck 2015 CMB data (Planck Collaboration 2016) do not require flat spatial hypersurfaces in the six parameter nonflat Λ CDM model.⁷ In the six parameter nonflat Λ CDM model, com-

pared to the six parameter flat- Λ CDM model, n_s is replaced by Ω_k . Park & Ratra (2018a) used the largest compilation of current reliable observational data to study the nonflat Λ CDM inflation model, confirming the results of Ooba et al. (2018a) and finding stronger evidence for nonflatness, 5.1σ , favoring a very slightly closed model. The CMB anisotropy measurements also do not demand flat spatial hypersurfaces in the seven parameter nonflat XCDM dynamical dark energy inflation parameterization (Ooba et al. 2018b). Here w is the seventh cosmological parameter and again n_s is replaced by Ω_k . In the simplest seven parameter nonflat ϕ CDM dynamical dark energy inflation model (Pavlov et al. 2013) — in which α is the seventh cosmological parameter with n_s replaced by Ω_k — Ooba et al. (2018c) (also see Park & Ratra 2018b) again found that CMB anisotropy observations do not require flat spatial geometry. In both the XCDM and ϕ CDM inflation cases the data also favor a very slightly closed model. All three slightly closed models are more consistent with σ_8 constraints from weak lensing observations.

In this paper we determine observational constraints on the seven parameter tilted flat-XCDM⁸ and the seven parameter untilted nonflat XCDM dynamical dark energy inflation parameterizations. For this purpose we use an updated version of the Planck 2015 CMB anisotropy, and (almost all currently available reliable) SNIa apparent magnitude, BAO distance, growth factor, and Hubble parameter data compilation of Park & Ratra (2018a). Our main update here is the replacement of the Joint Light-curve Analysis (JLA) compilation of apparent magnitude measurements of 740 SNIa (Betoule et al. 2014) by the Pantheon collection of 1048 SNIa measurements (Scolnic et al. 2017). When used with the Planck 2015 CMB anisotropy data in an analysis of the nonflat Λ CDM case, the Pantheon data place tighter constraints on spatial curvature than do the JLA data. Overall, for the full data compilation, our updated results for the tilted flat- Λ CDM inflation model and the nonflat Λ CDM inflation model here are very similar to those of Park & Ratra (2018a), with evidence for nonflatness in the nonflat Λ CDM case now becoming 5.2σ (from 5.1σ).

Our first main goal here is to examine the consequences of including a significant amount of recent, reliable, non-CMB data on the discovery of Ooba et al. (2018d) that the Planck 2015 CMB anisotropy data and a few BAO distance measurements favor the seven parameter tilted flat-XCDM parameterization over the six parameter standard flat- Λ CDM model. Our second main goal is to examine the effect that the inclusion of this new non-CMB data compilation has on the discovery of Ooba et al. (2018b) that the Planck 2015 CMB anisotropy observations and a few BAO distance measurements are not inconsistent with the closed-XCDM inflation parameterization. Our third main goal is to use this large compilation of reliable data to examine the compatibility of the cosmological constraints from each type of data and to also more tightly measure cosmological parameters than has been achieved to date, and in particular to also find out which model parameters can or cannot be measured from these data in a cosmological-model-independent manner.

⁵ While XCDM is widely used to model dynamical dark energy, it does not accurately model ϕ CDM (Podariu & Ratra 2001; Ooba et al. 2018d).

⁶ Both analyses also included in their data compilation a high value of H_0 estimated from the local expansion rate. We do not include this high local H_0 value in the data compilation we use here to constrain cosmological parameters, as it is not consistent with the other data we use, in the Λ CDM, XCDM, and ϕ CDM models.

⁷ Non-CMB observations do not tightly constrain spatial curvature (Farooq et al. 2015; Cai et al. 2016; Chen et al. 2016; Yu & Wang 2016; L’Huillier

& Shafieloo 2017; Farooq et al. 2017; Li et al. 2016; Wei & Wu 2017; Rana et al. 2017; Yu et al. 2018; Mitra et al. 2018, 2019; Ryan et al. 2018, 2019), except for a compilation of all of the most recent SNIa, BAO and Hubble parameter data, which also (mildly) favors closed spatial hypersurfaces (Park & Ratra 2018a) and for a compilation of primordial deuterium abundance measurements which favors a flat geometry (Penton et al. 2018).

⁸ For earlier constraints on the flat-XCDM model, see Zhao et al. (2007), Wang et al. (2007), Wang et al. (2009), and references therein.

We find that the seven parameter tilted flat- Λ CDM inflation parameterization continues to provide a better fit to the data than does the six parameter standard Λ CDM model. However, for the large compilation of data used here we find the Λ CDM dynamical dark energy case is only 0.28σ better than the standard Λ CDM case (compared to the 1.1σ Ooba et al. 2018d found with the smaller data compilation). This is not a significant improvement over the standard model but on the other hand the Λ CDM parameterization cannot be ruled out. Also in agreement with Ooba et al. (2018d) we do not find a deviation from $w = -1$ (a cosmological constant) for the flat- Λ CDM case.⁹ Similar to the Λ CDM models in Park & Ratra (2018a), the tilted flat- Λ CDM model continues to better fit the weak lensing bounds in the σ_8 - Ω_m plane than does the untilted nonflat Λ CDM model.

For the untilted nonflat Λ CDM inflation parameterization, our results here, determined using much more non-CMB data, are consistent with and strengthen those of Ooba et al. (2018b). For the full data compilation we now find a more than 3.4σ deviation from spatial flatness and now, for the first time, we also find a corresponding deviation from a cosmological constant with $w = -0.960 \pm 0.032$ in the nonflat Λ CDM case being more than 1.2σ away from the cosmological constant value of $w = -1$. The nonflat Λ CDM parameterization better fits the weak lensing limits in the σ_8 - Ω_m plane. For the full data combination we consider here (including CMB lensing data), we find that the observed low- ℓ CMB temperature and polarization anisotropy multipole number (ℓ) power spectrum C_ℓ is best fit¹⁰ by the tilted flat- Λ CDM model, followed by the tilted flat- Λ CDM parameterization, with the untilted nonflat Λ CDM model and the untilted nonflat Λ CDM parameterization in third and fourth place. The tilted flat- Λ CDM model and the tilted flat- Λ CDM parameterization best fit the observed higher- ℓ C_ℓ 's, followed by the untilted nonflat Λ CDM parameterization and the untilted nonflat Λ CDM model in third and fourth place.

We find that H_0 is measured in an almost model-independent manner with values that are consistent with most other estimates. However, as also found in Park & Ratra (2018a), some measured cosmological parameter values, including $\Omega_b h^2$, τ , and $\Omega_c h^2$, differ significantly between the flat and the nonflat models and so caution is needed when utilizing cosmological measurements of such parameters.

In Sec. 2 we briefly summarize the cosmological data we use in our analyses. In Sec. 3 we briefly summarize the methods we use for our analyses. The observational constraints resulting from these data for the tilted flat- Λ CDM and the nonflat Λ CDM inflation parameterizations are presented in Sec. 4. We conclude in Sec. 5.

2. DATA

As in Park & Ratra (2018a) we use the TT + lowP and TT + lowP + lensing Planck 2015 CMB anisotropy data (Planck

⁹ These results differ from those of earlier approximate analyses, based on less and less reliable data than we have used here (Solà et al. 2017a, 2018, 2017b,c,d; Gómez-Valent & Solà 2017, 2018), that favor the flat- Λ CDM case over the flat- Λ CDM one by 3σ or greater and find w deviating from -1 by more than 3σ .

¹⁰ Here by best fit we mean that the corresponding model has the lowest χ^2 of the models under consideration. As discussed elsewhere and below, a number of these models are not nested and the Planck 2015 data number of degrees of freedom are ambiguous, so in many cases it is not possible to convert the $\Delta\chi^2$'s we compute here to a quantitative goodness of fit and so many of our statements here about goodness of fit are qualitative. See below for more detailed discussion of this issue.

Collaboration 2016). Here TT denotes the low- ℓ ($2 \leq \ell \leq 29$) and high- ℓ ($30 \leq \ell \leq 2508$; PlikTT) Planck 2015 temperature-only C_ℓ^{TT} data and lowP represents low- ℓ polarization C_ℓ^{TE} , C_ℓ^{EE} , and C_ℓ^{BB} power spectra measurements at $2 \leq \ell \leq 29$. The collection of low- ℓ temperature and polarization measurements is referred to as lowTEB. The CMB lensing data we use is the power spectrum of the lensing potential measured by Planck.

Instead of using the JLA apparent magnitude measurement compilation of 740 SNIa (Betoule et al. 2014), we use the Pantheon collection of 1048 SNIa apparent magnitude measurements over the broader redshift range of $0.01 < z < 2.3$ (Scolnic et al. 2017), which includes 276 SNIa ($0.03 < z < 0.65$) discovered by the Pan-STARRS1 Medium Deep Survey and SNIa distance estimates from SDSS, SNLS and low- z HST samples. Throughout this paper, we use the abbreviation SN to denote the Pantheon SNIa sample.

We make one change to the BAO compilation of Sec. 2.3 and Table 1 of Park & Ratra (2018a), here using $D_V(r_{d,\text{fid}}/r_d) = 3843 \pm 147$ Mpc for the Ata et al. (2018) BAO data point, instead of the old value, $D_V(r_{d,\text{fid}}/r_d) = 3855 \pm 170$ Mpc, given in the initial version of their preprint (arXiv:1705.06373v1). See Sec. 2.3 of Park & Ratra (2018a) for the definitions of the above expressions. Throughout this paper, we use the abbreviation BAO to denote this updated BAO compilation.

We also use the same Hubble parameter, $H(z)$, and growth rate, $f(z)\sigma_8(z)$, measurements listed in Tables 2 and 3 of Park & Ratra (2018a). More precisely, Table 2 of Park & Ratra (2018a) lists all more reliable cosmic chronometric $H(z)$ data (31 measurements in all), while Table 1 of Park & Ratra (2018a) includes three radial BAO $H(z)$ measurements.

3. METHODS

We use the publicly available CAMB/COSMOMC analysis software (November 2016 version) (Challinor & Lasenby 1999; Lewis et al. 2000; Lewis & Bridle 2002) to constrain cosmological parameters of the tilted flat and the untilted nonflat Λ CDM dynamical dark energy inflation parameterizations with Planck 2015 CMB measurements and non-CMB data sets. We use the CAMB Boltzmann code to compute the angular power spectra for CMB temperature fluctuations, polarization, and lensing potential, and COSMOMC, based on the Markov chain Monte Carlo (MCMC) method, to determine the range of model parameters favored by the data. We use the same COSMOMC settings adopted in Planck Collaboration (2016) and used in Park & Ratra (2018a).

The spatially-flat tilted Λ CDM inflation case primordial power spectrum (Lucchin & Matarrese 1985; Ratra 1992, 1989) is

$$P(k) = A_s \left(\frac{k}{k_0} \right)^{n_s}, \quad (1)$$

where A_s is the amplitude of the power spectrum at the pivot scale $k_0 = 0.05 \text{ Mpc}^{-1}$ and k is wavenumber. The untilted nonflat Λ CDM inflation case primordial power spectrum (Ratra & Peebles 1995; Ratra 2017) is

$$P(q) \propto \frac{(q^2 - 4K)^2}{q(q^2 - K)}, \quad (2)$$

which reduces to the $n_s = 1$ spectrum in the spatially-flat limit ($K = 0$). For scalar perturbations, $q = \sqrt{k^2 + K}$ is wavenumber where $K = -(H_0^2/c^2)\Omega_k$ is spatial curvature and c is the

speed of light. In the spatially-closed model, with negative Ω_k , normal modes are characterized by positive integers $\nu = qK^{-1/2} = 3, 4, 5, \dots$. We use $P(q)$ as the initial spatial inhomogeneity perturbation power spectrum for the nonflat model by normalizing it at the pivot scale k_0 to the value of A_s .

Our analyses methods are very similar to those described in Sec. 3.2 of [Park & Ratra \(2018a\)](#). During the MCMC process we set the same priors for the cosmological parameters as in [Park & Ratra \(2018a\)](#). For the seventh parameter w , we set $-3 \leq w \leq 0.2$. In our analyses with the Pantheon SNIa sample, we do not set priors for the nuisance parameters (α_{SN} and β_{SN}) related to the stretch and the color correction of the SNIa light curves, since the stretch and color parameters of the Pantheon SNIa used here are set to zero.¹¹

4. OBSERVATIONAL CONSTRAINTS

We first examine how much more effective the improved Pantheon SNIa data are in constraining cosmological parameters, relative to the JLA data. Figure 1 compares the likelihood distributions of the model parameters for the JLA and the Pantheon data sets, in conjunction with the CMB observations, for the spatially-flat tilted and for the untilted nonflat Λ CDM inflation models. The mean and 68.3% confidence limits of model parameters are presented in Table 1.¹² Without CMB lensing data, the Pantheon data are a little more constraining than the JLA data. When CMB lensing data are included, the largest reduction in error bars occur for the nonflat Λ CDM case, where the error bars for Ω_m , H_0 , and Ω_k are approximately only 80% as large for the CMB + Pantheon combination when compared to the CMB + JLA case. From this Table we also see that including CMB lensing measurements results in a decrease of A_s and τ in both models.

Note that our six parameter physically-consistent untilted non-power-law power spectrum nonflat Λ CDM model constrained by the CMB and Pantheon data favors nonflat geometry and that the parameter constraints determined using our model are quite different from those presented in [Scolnic et al. \(2017\)](#) that were derived using the seven parameter physically-inconsistent tilted power-law power spectrum nonflat Λ CDM model (with varying spectral index n_s) which were found to favor spatial flatness ($\Omega_k = 0.004 \pm 0.006$, $\Omega_m = 0.295 \pm 0.024$, $H_0 = 69.695 \pm 2.933$ km s⁻¹ Mpc⁻¹ for the TT + lowP + Pantheon data combination).

Table 2 lists the parameter constraints for the tilted spatially-flat and for the untilted nonflat Λ CDM inflation models, for the updated complete data set we use here. These constraints can be compared to those listed in the bottom right panels of Tables 5–8 of [Park & Ratra \(2018a\)](#) that were derived using the JLA SNIa data and the initial preprint value of the [Ata et al. \(2018\)](#) BAO distance measurement. There are very small differences between the constraints derived using

¹¹ In addition to α_{SN} and β_{SN} , the distance moduli of the Pantheon SNIa are affected by three more nuisance parameters, the absolute B -band magnitude (M_B), the distance correction based on the host-galaxy mass (Δ_M), and the distance correction based on predicted biases from simulation (Δ_B) ([Scolnic et al. 2017](#)). Consequently, the number of degrees of freedom of the Pantheon sample is less than the number of SNIa. For example, for a flat- Λ CDM model analysis that fits Ω_m , the number of degrees of freedom becomes 1042 (= 1048–6).

¹² The parameter values of the tilted flat- Λ CDM model constrained by using TT + lowP (+lensing) + JLA data are in good agreement with the Planck results. See Planck 2015 cosmological parameter tables `base_plikHM_TT_lowTEB_post_JLA` for TT + lowP + JLA data and `base_plikHM_TT_lowTEB_lensing_post_JLA` for TT + lowP + lensing + JLA data ([Planck Collaboration 2015](#)).

our previous and our updated full data sets.

Our results for the tilted flat and the nonflat XCDM parameterizations are presented in Figs. 2–5 and Tables 3–6. In the plots we omit likelihood contours for TT + lowP (+ lensing) + SN + BAO data (excluding or including the Planck 2015 CMB lensing data) in both tilted flat and nonflat XCDM cases because they are very similar to those for TT + lowP (+ lensing) + SN + BAO + $H(z)$ data.

The entries for the tilted flat-XCDM parameterization in the TT + lowP panel of Table 3 and in the TT + lowP + lensing panel in Table 4 are very consistent with the corresponding Table 1 entries of [Ooba et al. \(2018d\)](#), except for those for w , H_0 , Ω_m , and σ_8 . This is because [Ooba et al. \(2018d\)](#) use a flat prior non-zero over $0.2 \leq h \leq 1.3$ for H_0 while we use a flat prior non-zero over $0.2 \leq h \leq 1$.¹³ The entries for the nonflat XCDM parameterization in the TT + lowP panel of Table 5 and in the TT + lowP + lensing panel in Table 6 agree well with the corresponding entries in Table 1 of [Ooba et al. \(2018b\)](#). [Ooba et al. \(2018b\)](#) and [Ooba et al. \(2018d\)](#) compute the C_ℓ 's using CLASS ([Blas et al. 2011](#)) and performed the MCMC analyses with Monte Python ([Audren et al. 2013](#)), so it is reassuring that our results agree well with their results. Our estimates of w , Ω_m , and H_0 for the tilted flat-XCDM parameterization from the TT + lowP + SN data agree very well with the values presented in [Scolnic et al. \(2017\)](#), $w = -1.031 \pm 0.040$, $\Omega_m = 0.306 \pm 0.012$, and $H_0 = 68.335 \pm 1.098$ km s⁻¹ Mpc⁻¹, which provides another reassuring check on our analyses.

From Tables 3 and 4 we see that, when they are added to the Planck CMB anisotropy observations, for the tilted flat-XCDM case, the BAO measurements mostly prove more restrictive than either the SN, $H(z)$, or $f\sigma_8$ data, except for w where the SN data are more restrictive than the BAO data. However, when the CMB lensing data are included, Table 4, the CMB + SN limits on w , H_0 , and σ_8 are more restrictive than those from the CMB data combined with BAO, or $H(z)$, or $f\sigma_8$ measurements, while all four non-CMB data sets used in conjunction with the CMB data provide equally restrictive constraints on $\Omega_b h^2$ and A_s .¹⁴ We note that our BAO compilation includes radial $H(z)$ measurements and the $f\sigma_8$ data of [Alam et al. \(2017\)](#). It is likely that if these are moved to the $H(z)$ and $f\sigma_8$ data sets, CMB and BAO, SN, $H(z)$, or $f\sigma_8$ constraints will all be about equally restrictive for the flat-XCDM parameterization.

The nonflat XCDM case is more interesting. When CMB lensing data are included, Table 6, CMB data with either SN, or BAO, or $H(z)$, or $f\sigma_8$ data, provide approximately equally restrictive constraints on $\Omega_b h^2$, $\Omega_c h^2$, and θ_{MC} , while CMB + BAO data provide the tightest constraints on τ , A_s , Ω_k , H_0 , Ω_m , and σ_8 , with CMB + SN setting tightest limits on w .¹⁵

¹³ Since the flat prior on h adopted here is the same as in the Planck team's analyses, the parameters for the tilted flat-XCDM case constrained with TT + lowP (+lensing) agree with the Planck results. See `base_w_plikHM_TT_lowTEB` for TT + lowP data and `base_w_plikHM_TT_lowTEB_post_lensing` for TT + lowP + lensing data ([Planck Collaboration 2015](#)).

¹⁴ This is not the case in the tilted flat- Λ CDM model, where for the data set including the CMB lensing data, the CMB + BAO constraints on all parameters are more restrictive than those determined by combining the CMB data with either the SN, or $H(z)$, or $f\sigma_8$ measurements. For this model we show only the CMB + SN constraints in Table 1.

¹⁵ In the nonflat Λ CDM model (results mostly not shown here, except for CMB + SN shown in Table 1), $\Omega_b h^2$, $\Omega_c h^2$, and θ_{MC} are about equally well constrained by any of the four non-CMB data sets when used with the CMB (including lensing) data, with CMB + BAO setting tighter limits on τ , A_s , Ω_k ,

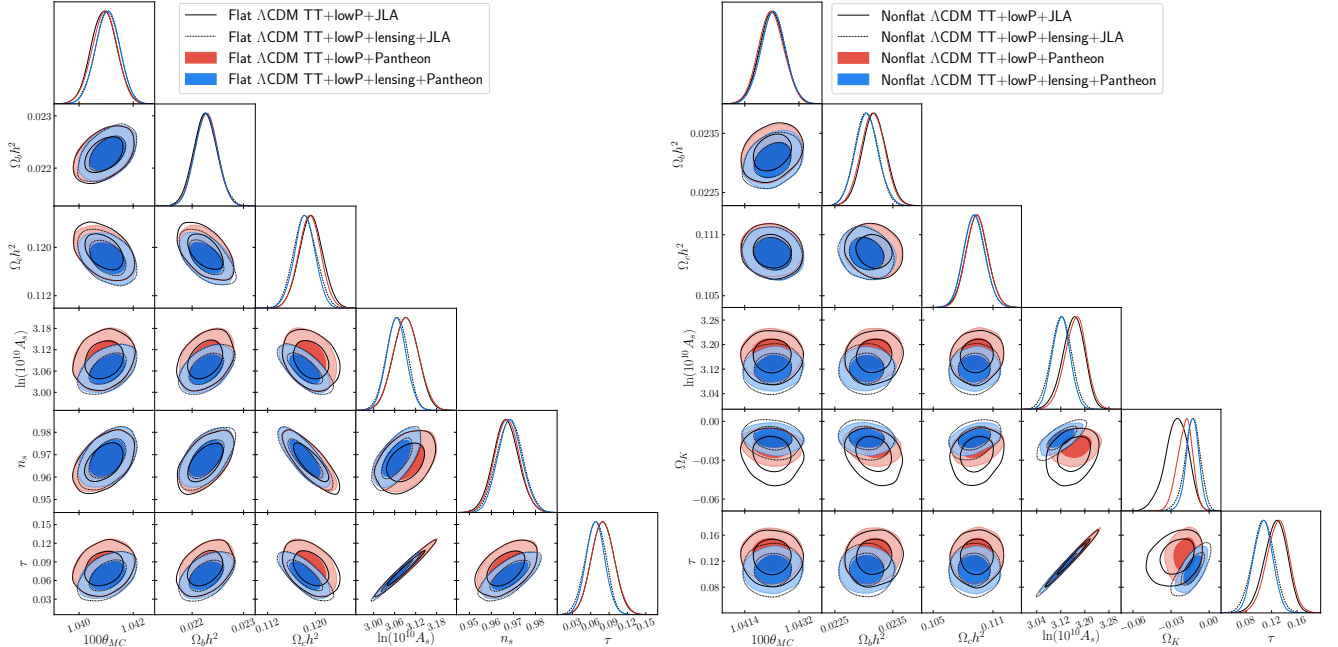


Figure 1. Likelihood distributions of the tilted flat (left) and untilted nonflat (right) Λ CDM inflation model parameters favored by the Planck CMB TT + lowP (+ lensing) and SNIa data. Here the parameter constraints are compared for the JLA SNIa data and the Pantheon SNIa data and summarized in Table 1. Two-dimensional marginalized likelihood contours as well as one-dimensional likelihoods are shown as solid and dashed black curves for JLA and filled contours and colored curves for Pantheon data.

Table 1

Mean and 68.3% confidence limits of tilted flat and untilted nonflat Λ CDM model parameters constrained by Planck and SNIa data. JLA versus Pantheon.

Tilted flat- Λ CDM model				
Parameter	TT+lowP+JLA	TT+lowP+lensing+JLA	TT+lowP+Pantheon	TT+lowP+lensing+Pantheon
$\Omega_b h^2$	0.02226 ± 0.00023	0.02227 ± 0.00022	0.02228 ± 0.00022	0.02228 ± 0.00022
$\Omega_c h^2$	0.1193 ± 0.0020	0.1183 ± 0.0019	0.1191 ± 0.0019	0.1182 ± 0.0017
$100\theta_{MC}$	1.04092 ± 0.00047	1.04105 ± 0.00045	1.04094 ± 0.00046	1.04106 ± 0.00044
τ	0.080 ± 0.019	0.068 ± 0.016	0.080 ± 0.019	0.068 ± 0.015
$\ln(10^{10} A_s)$	3.092 ± 0.035	3.066 ± 0.029	3.092 ± 0.036	3.065 ± 0.028
n_s	0.9666 ± 0.0057	0.9683 ± 0.0058	0.9671 ± 0.0056	0.9684 ± 0.0055
H_0 [km s $^{-1}$ Mpc $^{-1}$]	67.52 ± 0.89	67.93 ± 0.88	67.62 ± 0.84	67.96 ± 0.80
Ω_m	0.312 ± 0.012	0.306 ± 0.012	0.311 ± 0.011	0.306 ± 0.011
σ_8	0.829 ± 0.014	0.8156 ± 0.0093	0.829 ± 0.015	0.8152 ± 0.0094
Untilted nonflat Λ CDM model				
Parameter	TT+lowP+JLA	TT+lowP+lensing+JLA	TT+lowP+Pantheon	TT+lowP+lensing+Pantheon
$\Omega_b h^2$	0.02318 ± 0.00020	0.02304 ± 0.00020	0.02316 ± 0.00020	0.02305 ± 0.00020
$\Omega_c h^2$	0.1094 ± 0.0011	0.1091 ± 0.0011	0.1094 ± 0.0011	0.1091 ± 0.0011
$100\theta_{MC}$	1.04231 ± 0.00042	1.04233 ± 0.00041	1.04228 ± 0.00042	1.04235 ± 0.00041
τ	0.126 ± 0.018	0.107 ± 0.017	0.130 ± 0.018	0.107 ± 0.015
$\ln(10^{10} A_s)$	3.162 ± 0.036	3.121 ± 0.034	3.169 ± 0.035	3.121 ± 0.030
Ω_k	-0.0257 ± 0.0091	-0.0133 ± 0.0062	-0.0192 ± 0.0060	-0.0132 ± 0.0051
H_0 [km s $^{-1}$ Mpc $^{-1}$]	61.5 ± 2.9	66.0 ± 2.5	63.6 ± 2.2	66.0 ± 2.0
Ω_m	0.355 ± 0.033	0.306 ± 0.023	0.330 ± 0.022	0.306 ± 0.018
σ_8	0.815 ± 0.018	0.805 ± 0.017	0.822 ± 0.017	0.805 ± 0.015

Table 2
Tilted flat and untilted nonflat Λ CDM model parameters constrained with Planck, SN, BAO, $H(z)$, and $f\sigma_8$ data (mean and 68.3% confidence limits).

Tilted flat- Λ CDM model		
Parameter	TT+lowP+SN+BAO+ $H(z)$ + $f\sigma_8$	TT+lowP+lensing+SN+BAO+ $H(z)$ + $f\sigma_8$
$\Omega_b h^2$	0.02233 ± 0.00020	0.02232 ± 0.00019
$\Omega_c h^2$	0.1178 ± 0.0011	0.1177 ± 0.0011
$100\theta_{MC}$	1.04104 ± 0.00042	1.04108 ± 0.00041
τ	0.070 ± 0.017	0.066 ± 0.012
$\ln(10^{10} A_s)$	3.069 ± 0.033	3.061 ± 0.023
n_s	0.9693 ± 0.0042	0.9692 ± 0.0043
H_0 [km s $^{-1}$ Mpc $^{-1}$]	68.15 ± 0.52	68.19 ± 0.50
Ω_m	0.3031 ± 0.0067	0.3025 ± 0.0064
σ_8	0.815 ± 0.013	0.8117 ± 0.0088
Untilted nonflat Λ CDM model		
Parameter	TT+lowP+SN+BAO+ $H(z)$ + $f\sigma_8$	TT+lowP+lensing+SN+BAO+ $H(z)$ + $f\sigma_8$
$\Omega_b h^2$	0.02307 ± 0.00020	0.02305 ± 0.00019
$\Omega_c h^2$	0.1094 ± 0.0010	0.1093 ± 0.0010
$100\theta_{MC}$	1.04225 ± 0.00042	1.04227 ± 0.00041
τ	0.121 ± 0.016	0.112 ± 0.012
$\ln(10^{10} A_s)$	3.150 ± 0.033	3.132 ± 0.022
Ω_k	-0.0083 ± 0.0016	-0.0083 ± 0.0016
H_0 [km s $^{-1}$ Mpc $^{-1}$]	67.96 ± 0.62	68.01 ± 0.62
Ω_m	0.2882 ± 0.0055	0.2875 ± 0.0055
σ_8	0.820 ± 0.014	0.8121 ± 0.0095

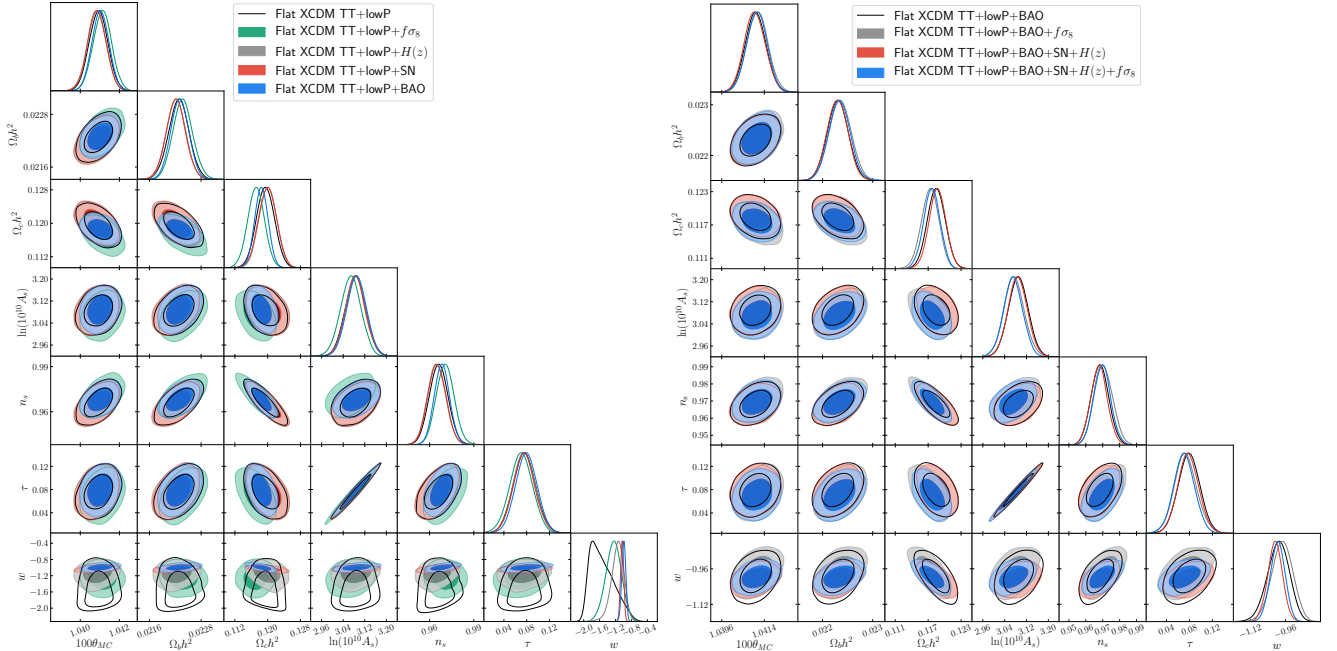


Figure 2. Likelihood distributions of the tilted flat-XCDM model parameters constrained by Planck CMB TT + lowP, SN, BAO, $H(z)$, and $f\sigma_8$ data. Two-dimensional marginalized likelihood contours as well as one-dimensional likelihoods are shown for cases when each non-CMB measurement set is added to the Planck TT + lowP data (left panel) and when the Hubble parameter, SN, growth rate data, and the combination of them, are added to TT + lowP + BAO data (right panel). For clarity the TT + lowP (left) and TT + lowP + BAO (right panel) cases are shown as solid black curves.

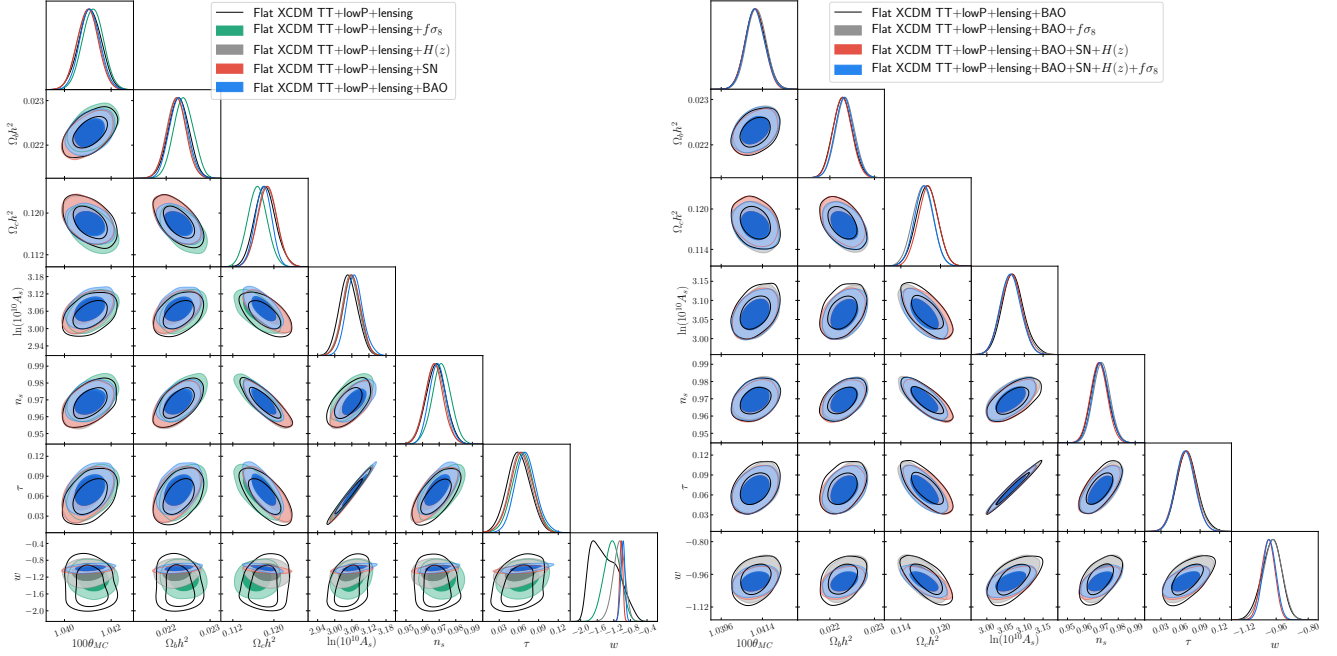


Figure 3. Same as Fig. 2 but now also including the Planck CMB lensing measurements.

Focusing on the CMB TT + lowP + lensing measurements, Figs. 3 and 5 and Tables 4 and 6, we see that adding each of the four non-CMB measurement sets at a time to the CMB data (left triangle plots in both figures) produces four sets of contours that are quite mutually consistent, as well as consistent with the original CMB only contours, for both the tilted flat-XCDM parameterization and for the untilted nonflat XCDM parameterization. It is reassuring that the four sets of non-CMB measurements do not push the CMB constraints in significantly different directions. This is also the case for the tilted flat-XCDM parameterization when the CMB lensing data are excluded (left triangle plot of Fig. 2). However, in the untilted nonflat XCDM case excluding the lensing data when any of the four sets of non-CMB observations are added to the CMB measurements (left triangle panel of Fig. 4), they each push the results toward a smaller $|\Omega_k|$ (closer to spatially flat) and a slightly larger τ and A_s and a smaller $\Omega_b h^2$ than what is favored by the CMB measurements alone, though all five sets of constraint contours are mostly mutually consistent. However, there is tension between the TT + lowP + SN and the TT + lowP + BAO contours in the Ω_k - w plane (Fig. 4 left and Table 5), where CMB + SN data give constraints on Ω_k and w that deviate from the CMB + BAO data values by over 2σ , with w also deviating from the cosmological constant ($w = -1$) by over 2σ for the CMB + SN case and Ω_k differing from 0 by more than 3σ in both cases.

While adding the BAO data to the CMB data usually results in the biggest difference, the other three non-CMB sets of data also contribute. Focusing on TT + lowP + lensing data, we see from Table 4 for the tilted flat-XCDM parameterization that the BAO data tightly constrains model parameters, especially $\Omega_c h^2$, while the $f\sigma_8$ measurements push $\Omega_b h^2$ and n_s to larger values and push $\Omega_c h^2$ to a smaller value. In this case H_0 is the parameter whose error bar is decreased the most for the full combination of data relative to the CMB + SN data combination, followed by the Ω_m error bar reduction relative to CMB + BAO data combination. For the untilted nonflat

XCDM case, from Table 6, the error bars that shrink the most when CMB (including lensing) data are used in conjunction with the four non-CMB data sets are those on w (relative to the CMB + SN case) and H_0 and Ω_m (relative to the CMB + BAO combination).

Continuing to focus on the TT + lowP + lensing data, Tables 4 and 6, we see that for the tilted flat-XCDM parameterization, adding the four sets of non-CMB data to the mix most influences σ_8 , w , and Ω_m , with the σ_8 central value moving down by 1.3σ and the w and Ω_m central values moving up by 1.3σ and 1.2σ , all of the CMB data alone error bars; θ_{MC} is hardly affected by adding the four non-CMB data sets, changing by only 0.042σ . The situation for the nonflat XCDM parameterization is a little less dramatic, with $\ln(10^{10} A_s)$, and τ central values increasing by 0.91σ and 0.86σ of the CMB data alone error bars, and Ω_k moving closer to flatness by 0.71σ ; the $\Omega_b h^2$ central value does not change in this case.

Figure 6 shows marginalized likelihood contours in the Ω_m - w plane for the tilted flat-XCDM parameterization and in the w - Ω_k plane for the untilted nonflat XCDM case. For CMB TT + lowP + lensing data combined with the non-CMB data sets, the flat-XCDM parameterization prefers $w = -1$, favoring the cosmological constant as dark energy. On the other hand, the nonflat XCDM parameterization, when constrained by the full data, prefers closed spatial hypersurfaces and a dark energy equation of state parameter $w > -1$.

More precisely, including the four non-CMB sets of measurements in the mix, we find in the tilted flat-XCDM parameterization (bottom right panel of Table 4) that $w = -0.994 \pm 0.033$, which is more tightly restricted to $w = -1$ and the cosmological constant than the original Ooba et al. (2018d) finding of $w = -1.03 \pm 0.07$ (the last column of their Table 1).¹⁶

On the other hand, and perhaps the most striking conse-

¹⁶ These results differ from those of earlier approximate analyses, based on less and less reliable data, that indicated evidence for w deviating from -1 by more than 3σ (Solà et al. 2017a, 2018, 2017b,c,d; Gómez-Valent & Solà 2017, 2018).

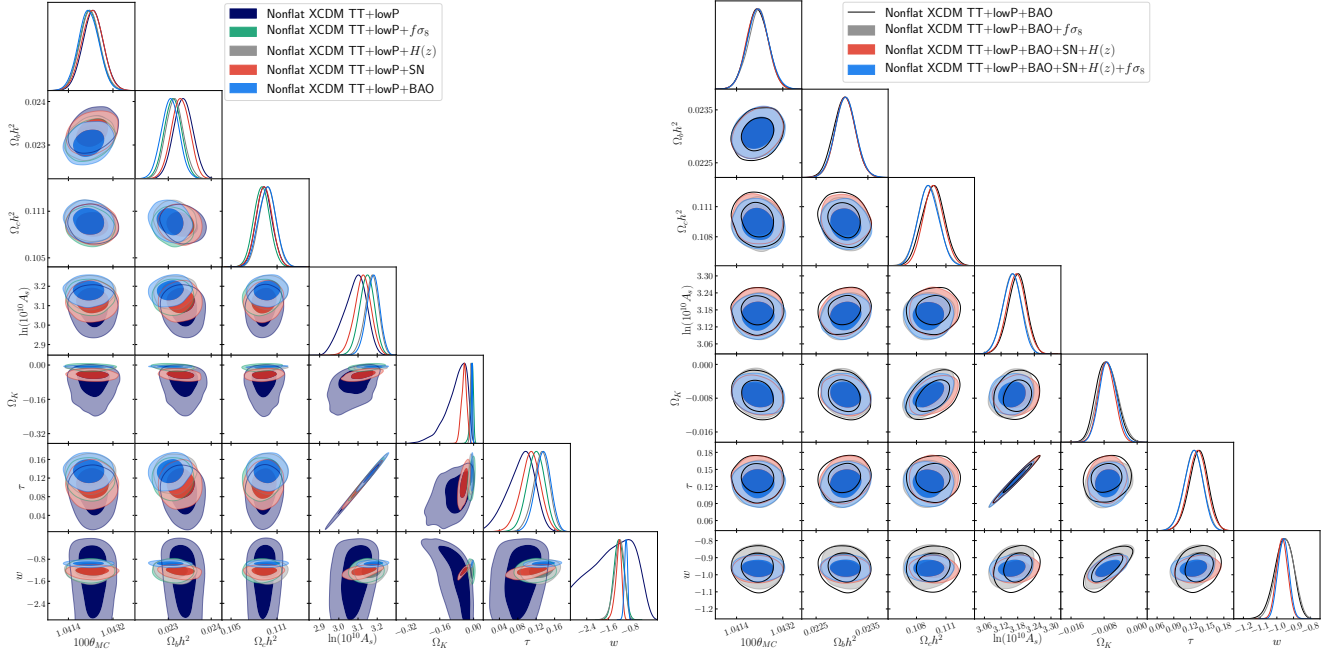


Figure 4. Likelihood distributions of the untilted nonflat XCDM model parameters constrained by Planck CMB TT + lowP, SN, BAO, $H(z)$, and $f\sigma_8$ data. Two-dimensional marginalized likelihood contours as well as one-dimensional likelihoods are shown for cases when each non-CMB measurement set is added to the Planck TT + lowP data (left panel) and when the Hubble parameter, growth rate data, and the combination of them, are added to TT + lowP + BAO data (right panel). For clarity, the result of TT + lowP + BAO is shown as solid black curves in the right panel.

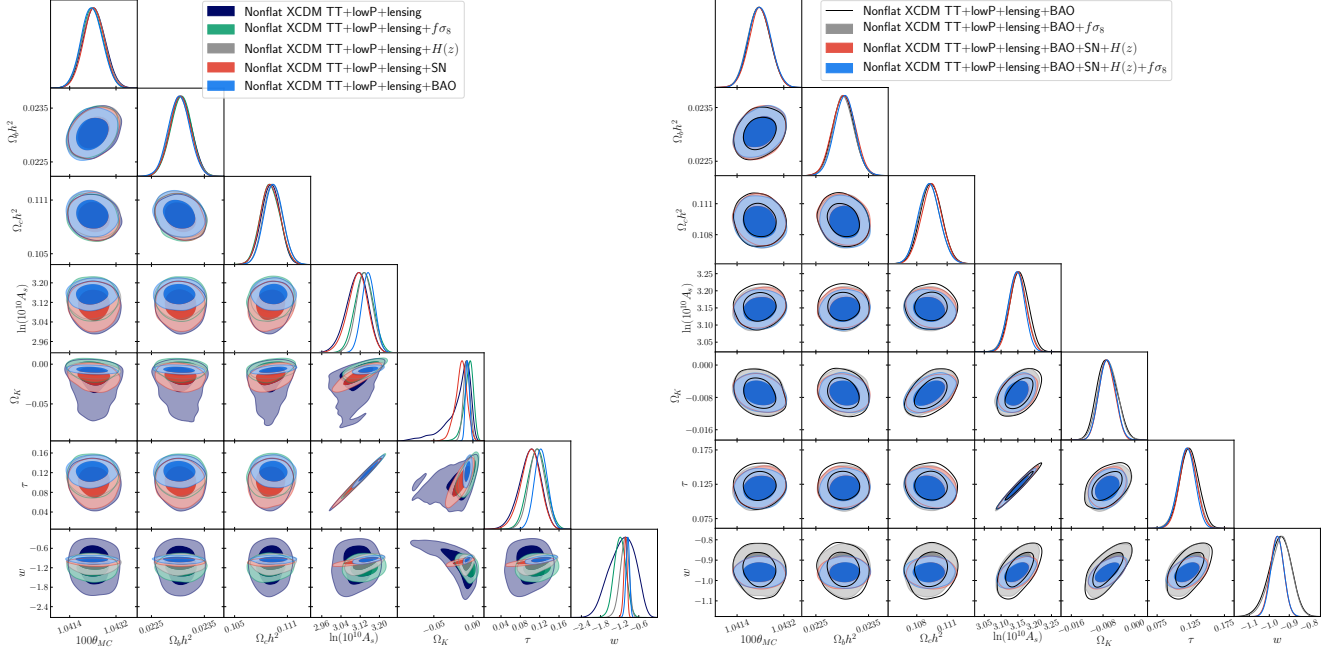


Figure 5. Same as Fig. 4 but now also including the Planck CMB lensing data.

quence of adding the four non-CMB data sets to the mix here, is the significant strengthening of the support for non-flatness in the untilted nonflat XCDM case, with it increasing to $\Omega_k = -0.0069 \pm 0.0020$, more than 3.4σ away from flatness now, for the full data combination in the bottom right panel of Table 6, compared to the 1.1σ from flatness for the CMB only case. That is now accompanied for the first time by mild evidence favoring dynamical dark energy with $w = -0.960 \pm 0.032$ that is more than 1.2σ away from

the cosmological constant. These results are consistent with but strengthen those of Ooba et al. (2018b) who found $\Omega_k = -0.008 \pm 0.003$ and $w = -1.00 \pm 0.10$ from Planck 2015 CMB anisotropy data in combination with a few BAO distance measurements. The stronger results here are driven in part by each of the four non-CMB data sets. CMB + BAO, CMB + SN, and CMB + $H(z)$ favor negative Ω_k values 2.8σ , 2.0σ , and 1.9σ away from flat, while CMB + $f\sigma_8$ and CMB + BAO favor w values that are 1.1σ more negative and 1σ less negative than

$w = -1$. On the other hand, CMB + $f\sigma_8$ data are consistent with a flat model and CMB + SN and CMB + $H(z)$ are consistent with the cosmological constant and $w = -1$. In favoring a closed model with w less negative than -1 , the BAO data play the most important role amongst the four non-CMB data sets.

For the full data combination (including CMB lensing data) in Tables 4 and 6, H_0 values measured using the tilted flat- Λ CDM and the nonflat Λ CDM parameterizations, 68.06 ± 0.77 and $67.45 \pm 0.75 \text{ km s}^{-1} \text{ Mpc}^{-1}$, are consistent with each other to within 0.57σ (of the quadrature sum of the two error bars).¹⁷ These values are very compatible with the median statistics estimate $H_0 = 68 \pm 2.8 \text{ km s}^{-1} \text{ Mpc}^{-1}$ (Chen & Ratra 2011a), which agrees with earlier median statistics measurements (Gott et al. 2001; Chen et al. 2003). Other recent measurements of H_0 are also very compatible with these estimates (Aubourg et al. 2015; Planck Collaboration 2016; Semiz & Çamlıbel 2015; L’Huillier & Shafieloo 2017; Chen et al. 2017; Luković et al. 2016; Wang et al. 2017; Lin & Ishak 2017; DES Collaboration 2017; Yu et al. 2018; Haridasu et al. 2018; Zhang et al. 2018; Gómez-Valent & Amendola 2018), but, as well known, these estimates are lower than the local expansion rate measurement of $H_0 = 73.48 \pm 1.66 \text{ km s}^{-1} \text{ Mpc}^{-1}$ (Riess et al. 2018).¹⁸

In our analyses here, H_0 and σ_8 (see below) are the only cosmological parameters that are measured in an almost cosmological model (tilt and spatial curvature) independent way. Measurements of other cosmological parameters determined using the two Λ CDM parameterizations differ more significantly. More precisely, measurements determined using the full data set (including CMB lensing) of w , Ω_m , θ_{MC} , $\ln(10^{10}A_s)$, $\Omega_b h^2$, τ , and $\Omega_c h^2$, differ by 0.74σ , 1.1σ , 2.0σ , 2.3σ , 2.5σ , 2.7σ , and 4.8σ (of the quadrature sum of both error bars). For some of these parameters, especially $\Omega_c h^2$ as well as probably τ and $\Omega_b h^2$, the cosmological model dependence of the measurement creates a much larger uncertainty than does the statistical error in a given cosmological model. This effect was first noticed in a comparison between measurements made using the tilted flat- Λ CDM and the untilted nonflat Λ CDM inflation models (Park & Ratra 2018a). From Tables 4 and 6, for the full data compilation (including CMB lensing), we find in the tilted flat- Λ CDM (nonflat Λ CDM) case $0.038 \leq \tau \leq 0.098$ ($0.095 \leq \tau \leq 0.143$) and $0.02191 \leq \Omega_b h^2 \leq 0.02275$ ($0.02265 \leq \Omega_b h^2 \leq 0.02345$) at 2σ , which are almost completely disjoint. It is not yet possible to measure $\Omega_c h^2$, τ , or $\Omega_b h^2$ (and possibly some other cosmological parameters as well) in a model independent way by using cosmological data.

For the full data combination (including CMB lensing data), σ_8 ’s measured using the two Λ CDM parameterizations, Tables 4 and 6, agree to 0.32σ (of the quadrature sum of the two error bars). Figures 7 and 8 show the marginalized two-dimensional likelihood distribution contours in the Ω_m – σ_8 plane for the tilted flat and untilted nonflat Λ CDM parameterizations constrained using the CMB and non-CMB data. For comparison we also plot the Λ CDM constraints obtained from a joint analysis of galaxy clustering and weak gravi-

tational lensing first year data of the Dark Energy Survey (DES Y1 All) (DES Collaboration 2018), whose 1σ confidence ranges are $\Omega_m = 0.264_{-0.019}^{+0.032}$ and $\sigma_8 = 0.807_{-0.041}^{+0.062}$. The marginalized likelihood distribution contours in the Ω_m – σ_8 plane determined by adding each non-CMB measurement set to the Planck 2015 CMB observations are consistent with each other, except for the nonflat Λ CDM parameterization where the TT + lowP + SN contours almost do not overlap with contours derived using any of the other three non-CMB data sets with the TT + lowP data (Fig. 8 top left panel). As expected, the BAO data provide the most restrictive constraints among the four non-CMB data sets.

While the σ_8 constraints from the tilted flat and untilted nonflat Λ CDM analyses (allowing for and ignoring CMB lensing data) are similar to the DES Y1 All result, the Ω_m constraints here favor a larger value by about 1.2σ (of the quadrature sum of the two error bars) for the flat- Λ CDM case for the full data combination. We emphasize that the best-fit point for the nonflat Λ CDM parameterization constrained by using the Planck CMB measurements (including lensing) combined with all non-CMB observations enters well into the 1σ region of the DES Y1 All constraint contour (Fig. 8 lower right panel), unlike the tilted flat Λ CDM parameterization case (Fig. 7 lower right panel).

Table 7 lists χ^2 values for the best-fit tilted flat and untilted nonflat Λ CDM models. This is an updated version of Table 9 of Park & Ratra (2018a), for the updated data sets we use here. Table 8 lists the corresponding quantities for the tilted flat and the untilted nonflat Λ CDM parameterizations. The best-fit position in parameter space is determined from Powell’s minimization method that is an efficient algorithm to find the location of the minimum χ^2 . We use the COSMOMC program (with an option `action=2`) to implement this method.¹⁹ In these Tables we list the individual χ^2 contribution of each data set used to constrain model parameters. The total χ^2 is the sum of those of the high- ℓ CMB TT likelihood (χ^2_{PlkTT}), the low- ℓ CMB power spectra of temperature and polarization (χ^2_{lowTEB}), lensing (χ^2_{lensing}), SN (χ^2_{SN}), $H(z)$ ($\chi^2_{H(z)}$), BAO (χ^2_{BAO}), $f\sigma_8$ data ($\chi^2_{f\sigma_8}$), as well as the contribution from the foreground nuisance parameters (χ^2_{prior}). Due to the nonconventional normalization of the Planck CMB anisotropy data likelihoods, the number of Planck 2015 CMB degrees of freedom is ambiguous. Given that the number of degrees of freedom of the Planck 2015 CMB data is unavailable and that the absolute value of χ^2 is arbitrary, only χ^2 differences between two models are meaningful for the Planck CMB data. In Table 7, for the untilted nonflat Λ CDM model, we list $\Delta\chi^2$, the excess χ^2 relative to the value of the tilted flat- Λ CDM model constrained using the same combination of measurements. For the non-CMB observations, the numbers of degrees of freedom are 1042, 31, 15, 10 for the SN, $H(z)$, BAO, $f\sigma_8$ data sets, respectively, a total of 1098 degrees of freedom. The reduced χ^2 ’s for each of the non-CMB measurement sets are $\chi^2/\nu \lesssim 1$. There are 189 points in the Planck 2015 (binned angular power spectrum) TT + lowP data and 197 when the CMB lensing data are included.

Conclusions about the qualitative relative goodness of fit of the tilted flat and nonflat Λ CDM models drawn from the updated data here are not very different from those found ear-

¹⁷ Potential systematic errors that might affect the value of H_0 , ignored here, have been discussed by Addison et al. (2016) and Planck Collaboration (2017).

¹⁸ This local measurement is 2.9σ (3.3σ), of the quadrature sum of both error bars, higher than H_0 measured here using the tilted flat- Λ CDM (untilted nonflat Λ CDM) parameterization. Other local expansion rate estimates find slightly lower H_0 ’s with larger error bars (Rigault et al. 2015; Zhang et al. 2017b; Dhawan et al. 2018; Fernández Arenas et al. 2018).

¹⁹ Our χ^2 values presented here for the tilted flat- Λ CDM model constrained with TT + lowP data are similar to the Planck results ($\chi^2_{\text{PlkTT}} = 761.9$; $\chi^2_{\text{lowTEB}} = 10495.14$, $\chi^2_{\text{prior}} = 1.86$ with total $\chi^2 = 11258.91$; Planck Collaboration 2015).

Table 3
Tilted flat- Λ CDM model parameters constrained with Planck TT + lowP, SN, BAO, $H(z)$, and $f\sigma_8$ data (mean and 68.3% confidence limits).

Parameter	TT+lowP	TT+lowP+SN	TT+lowP+BAO
$\Omega_b h^2$	0.02228 ± 0.00023	0.02221 ± 0.00023	0.02231 ± 0.00021
$\Omega_c h^2$	0.1195 ± 0.0022	0.1200 ± 0.0022	0.1185 ± 0.0016
$100\theta_{MC}$	1.04093 ± 0.00048	1.04085 ± 0.00047	1.04103 ± 0.00044
τ	0.076 ± 0.020	0.076 ± 0.019	0.079 ± 0.019
$\ln(10^{10} A_s)$	3.086 ± 0.037	3.086 ± 0.037	3.090 ± 0.036
n_s	0.9662 ± 0.0063	0.9651 ± 0.0061	0.9684 ± 0.0052
w	-1.53 ± 0.30	-1.034 ± 0.040	-0.993 ± 0.050
H_0 [km s $^{-1}$ Mpc $^{-1}$]	> 63.5 (95.4% C.L.)	68.2 ± 1.1	67.6 ± 1.2
Ω_m	0.207 ± 0.057	0.307 ± 0.012	0.309 ± 0.010
σ_8	0.977 ± 0.084	0.838 ± 0.019	0.824 ± 0.019
Parameter	TT+lowP+ $H(z)$	TT+lowP+SN+BAO	TT+lowP+SN+BAO+ $H(z)$
$\Omega_b h^2$	0.02222 ± 0.00022	0.02229 ± 0.00021	0.02230 ± 0.00020
$\Omega_c h^2$	0.1200 ± 0.0021	0.1186 ± 0.0015	0.1187 ± 0.0015
$100\theta_{MC}$	1.04085 ± 0.00047	1.04098 ± 0.00044	1.04100 ± 0.00044
τ	0.075 ± 0.019	0.078 ± 0.018	0.078 ± 0.018
$\ln(10^{10} A_s)$	3.086 ± 0.037	3.088 ± 0.035	3.088 ± 0.036
n_s	0.9648 ± 0.0061	0.9677 ± 0.0051	0.9679 ± 0.0050
w	-1.15 ± 0.16	-1.006 ± 0.034	-1.007 ± 0.034
H_0 [km s $^{-1}$ Mpc $^{-1}$]	71.9 ± 4.8	67.97 ± 0.77	68.00 ± 0.77
Ω_m	0.280 ± 0.037	0.3066 ± 0.0076	0.3064 ± 0.0075
σ_8	0.872 ± 0.047	0.827 ± 0.016	0.828 ± 0.016
Parameter	TT+lowP+ $f\sigma_8$	TT+lowP+BAO+ $f\sigma_8$	TT+lowP+SN+BAO+ $H(z)$ + $f\sigma_8$
$\Omega_b h^2$	0.02238 ± 0.00023	0.02235 ± 0.00022	0.02234 ± 0.00021
$\Omega_c h^2$	0.1172 ± 0.0020	0.1173 ± 0.0016	0.1177 ± 0.0015
$100\theta_{MC}$	1.04113 ± 0.00047	1.04111 ± 0.00044	1.04109 ± 0.00043
τ	0.070 ± 0.020	0.073 ± 0.020	0.071 ± 0.018
$\ln(10^{10} A_s)$	3.068 ± 0.038	3.075 ± 0.037	3.071 ± 0.035
n_s	0.9706 ± 0.0061	0.9704 ± 0.0054	0.9697 ± 0.0050
w	-1.25 ± 0.20	-0.975 ± 0.048	-0.996 ± 0.034
H_0 [km s $^{-1}$ Mpc $^{-1}$]	76.8 ± 6.9	67.5 ± 1.1	68.07 ± 0.78
Ω_m	0.244 ± 0.045	0.3079 ± 0.0098	0.3037 ± 0.0075
σ_8	0.885 ± 0.056	0.809 ± 0.017	0.814 ± 0.015

lier (Park & Ratra 2018a) from the original data. For the nonflat Λ CDM case relative to the flat- Λ CDM model, we have $\Delta\chi^2 = 21$ for TT + lowP + lensing and the full non-CMB compilation (last column in the last row of Table 7). As discussed above and in Ooba et al. (2018a,b,c) and Park & Ratra (2018a,b), it is not clear how to convert this into a quantitative relative probability as the two six parameter cases are not nested (and the number of degrees of freedom of the Planck measurements is unavailable). It is clear however that the nonflat Λ CDM model does a worse job in fitting the higher- ℓ C_ℓ 's than it does in fitting the lower- ℓ ones. We note that there has been discussion about systematic differences between constraints determined using the higher- ℓ and the lower- ℓ Planck 2015 CMB data (Addison et al. 2016; Planck Collaboration 2017). In addition, in the context of the flat- Λ CDM model, there appear to be inconsistencies between the higher- ℓ Planck 2015 CMB anisotropy data and the South Pole Telescope CMB anisotropy data (Aylor et al. 2017). It is possible that, if real, when these differences are resolved this could result in a reduction of the $\Delta\chi^2$'s found here.

Table 8 lists χ^2 values for the best-fit tilted flat and untilted

nonflat XCDM parameterizations. In the last column we list $\Delta\chi^2$, the excess χ^2 of the seven parameter XCDM case over the value of the corresponding six parameter Λ CDM model constrained using the same combination of data sets. These models are nested; the seven parameter tilted flat-XCDM (untilted nonflat XCDM) parameterization reduces to the six parameter tilted flat- Λ CDM (untilted nonflat Λ CDM) model when $w = -1$. In this case the ambiguity in the number of Planck 2015 degrees of freedom is not an obstacle to converting the $\Delta\chi^2$ values to a relative goodness of fit. From $\sqrt{-\Delta\chi^2}$, for the full data set (including CMB lensing), for one additional free parameter, we find that the tilted flat-XCDM (untilted nonflat XCDM) parameterization is a 0.28σ (0.87σ) better fit to the data than is the tilted flat- Λ CDM (untilted nonflat Λ CDM) model. (We emphasize that nonflat Λ CDM does not fit the data as well as flat- Λ CDM, although the difference in the goodness of fit cannot yet be precisely quantified.) These results are consistent with those of Ooba et al. (2018d) and Ooba et al. (2018b).

Of all these four models, the tilted flat-XCDM parameterization best fits the combined data, but at a lower level of sig-

Table 4Tilted flat- Λ CDM model parameters constrained with Planck TT + lowP + lensing, SN, BAO, $H(z)$, and $f\sigma_8$ data (mean and 68.3% confidence limits).

Parameter	TT+lowP+lensing	TT+lowP+lensing+SN	TT+lowP+lensing+BAO
$\Omega_b h^2$	0.02229 ± 0.00023	0.02223 ± 0.00022	0.02229 ± 0.00022
$\Omega_c h^2$	0.1183 ± 0.0021	0.1187 ± 0.0019	0.1179 ± 0.0016
$100\theta_{MC}$	1.04110 ± 0.00048	1.04099 ± 0.00045	1.04110 ± 0.00044
τ	0.060 ± 0.017	0.064 ± 0.017	0.070 ± 0.016
$\ln(10^{10} A_s)$	3.048 ± 0.032	3.060 ± 0.030	3.070 ± 0.030
n_s	0.9681 ± 0.0060	0.9671 ± 0.0056	0.9692 ± 0.0052
w	-1.41 ± 0.32	-1.020 ± 0.039	-0.984 ± 0.050
H_0 [km s ⁻¹ Mpc ⁻¹]	> 60.1 (95.4% C.L.)	68.3 ± 1.1	67.6 ± 1.2
Ω_m	0.223 ± 0.068	0.303 ± 0.012	0.309 ± 0.010
σ_8	0.924 ± 0.085	0.820 ± 0.013	0.811 ± 0.014
Parameter	TT+lowP+lensing+ $H(z)$	TT+lowP+lensing+SN+BAO	TT+lowP+lensing+SN+BAO+ $H(z)$
$\Omega_b h^2$	0.02224 ± 0.00022	0.02227 ± 0.00021	0.02228 ± 0.00021
$\Omega_c h^2$	0.1187 ± 0.0019	0.1182 ± 0.0015	0.1181 ± 0.0015
$100\theta_{MC}$	1.04101 ± 0.00046	1.04105 ± 0.00043	1.04107 ± 0.00042
τ	0.063 ± 0.017	0.067 ± 0.015	0.068 ± 0.015
$\ln(10^{10} A_s)$	3.056 ± 0.030	3.064 ± 0.028	3.065 ± 0.028
n_s	0.9672 ± 0.0058	0.9681 ± 0.0050	0.9686 ± 0.0050
w	-1.08 ± 0.14	-1.001 ± 0.0034	-1.000 ± 0.033
H_0 [km s ⁻¹ Mpc ⁻¹]	70.4 ± 4.5	67.97 ± 0.77	70.00 ± 0.76
Ω_m	0.289 ± 0.037	0.3057 ± 0.0074	0.3052 ± 0.0073
σ_8	0.836 ± 0.038	0.815 ± 0.011	0.815 ± 0.011
Parameter	TT+lowP+lensing+ $f\sigma_8$	TT+lowP+lensing+BAO+ $f\sigma_8$	TT+lowP+lensing+SN+BAO+ $H(z)$ + $f\sigma_8$
$\Omega_b h^2$	0.02240 ± 0.00022	0.02234 ± 0.00021	0.02233 ± 0.00021
$\Omega_c h^2$	0.1168 ± 0.0019	0.1173 ± 0.0015	0.1175 ± 0.0014
$100\theta_{MC}$	1.04122 ± 0.00045	1.04114 ± 0.00042	1.04108 ± 0.00042
τ	0.066 ± 0.017	0.069 ± 0.016	0.068 ± 0.015
$\ln(10^{10} A_s)$	3.060 ± 0.030	3.066 ± 0.029	3.063 ± 0.027
n_s	0.9715 ± 0.0057	0.9702 ± 0.0050	0.9696 ± 0.0051
w	-1.24 ± 0.20	-0.979 ± 0.047	-0.994 ± 0.033
H_0 [km s ⁻¹ Mpc ⁻¹]	76.7 ± 7.0	67.7 ± 1.1	68.06 ± 0.77
Ω_m	0.244 ± 0.046	0.307 ± 0.010	0.3034 ± 0.0073
σ_8	0.877 ± 0.054	0.806 ± 0.013	0.810 ± 0.011

nificance than the 1.1σ of [Ooba et al. \(2018d\)](#), and not close to the 3 or 4σ significance found in earlier approximate analyses ([Solà et al. 2017a, 2018, 2017b,c,d](#); [Gómez-Valent & Solà 2017, 2018](#)). While the tilted flat- Λ CDM parameterization does not provide a significantly better fit to the data, current data cannot rule out dynamical dark energy.

Figures 9 and 10 show plots of the CMB high- ℓ TT, and the low- ℓ TT, TE, EE power spectra of the best-fit tilted flat and untilted nonflat Λ CDM dynamical dark energy inflation parameterizations, excluding and including the lensing data, respectively. The best-fit tilted flat- Λ CDM models favored by the Planck CMB and non-CMB data agree well with the observed CMB power spectra at all ℓ . However, similar to the nonflat Λ CDM case studied in [Park & Ratra \(2018a\)](#), the nonflat Λ CDM parameterization constrained by using the Planck 2015 CMB data and each non-CMB data set generally has a poorer fit to the low- ℓ EE anisotropy power spectrum while it better fits the low- ℓ TT anisotropy power spectrum (see the bottom left panel of Figs. 9 and 10). The shape of the best-fit C_ℓ power spectra of models relative to the Planck CMB data points are quite consistent with the χ^2 's listed in Table 8. For

example, the best-fit untilted nonflat Λ CDM parameterization constrained by using the TT + lowP + lensing and full non-CMB data sets has a low- ℓ EE power spectrum that deviates the most from the Planck data and the corresponding value of χ^2_{lowTEB} is larger than values from other non-CMB combinations.

Figure 11 shows the best-fit initial power spectra of scalar fractional energy density spatial inhomogeneity perturbations for the untilted nonflat Λ CDM parameterization constrained using the Planck TT + lowP (left) and TT + lowP + lensing (right panel) data in conjunction with other non-CMB data sets. The reduction in power at low q in the best-fit closed- Λ CDM inflation parameterization spatial inhomogeneity power spectra shown in Fig. 11 is partly responsible for the low- ℓ TT power reduction of the best-fit closed model C_ℓ 's (see the lower panels of Figs. 9 and 10) relative to the best-fit tilted flat model C_ℓ 's.²⁰ The case of the best-fit nonflat Λ CDM parameterization for the TT + lowP + SN data is the most dramatic one, consistent with the reduced low- ℓ TT

²⁰ Other effects, including both the usual and integrated Sachs-Wolfe effects, also affect the shape of the low- ℓ C_ℓ 's.

Table 5
Untilted nonflat Λ CDM model parameters constrained with Planck TT + lowP, SN, BAO, $H(z)$, and $f\sigma_8$ data (mean and 68.3% confidence limits).

Parameter	TT+lowP	TT+lowP+SN	TT+lowP+BAO
$\Omega_b h^2$	0.02335 ± 0.00022	0.02328 ± 0.00021	0.02305 ± 0.00021
$\Omega_c h^2$	0.1093 ± 0.0010	0.1093 ± 0.0011	0.1097 ± 0.0011
$100\theta_{MC}$	1.04240 ± 0.00042	1.04237 ± 0.00043	1.04222 ± 0.00042
τ	0.087 ± 0.029	0.107 ± 0.022	0.134 ± 0.017
$\ln(10^{10} A_s)$	3.083 ± 0.058	3.124 ± 0.044	3.178 ± 0.034
Ω_k	-0.084 ± 0.052	-0.045 ± 0.013	-0.0074 ± 0.0024
w	-1.45 ± 0.75	-1.23 ± 0.11	-0.959 ± 0.056
H_0 [km s $^{-1}$ Mpc $^{-1}$]	55 ± 14	58.6 ± 2.7	67.0 ± 1.2
Ω_m	0.52 ± 0.24	0.390 ± 0.035	0.297 ± 0.010
σ_8	0.82 ± 0.13	0.834 ± 0.019	0.820 ± 0.020
Parameter	TT+lowP+ $H(z)$	TT+lowP+SN+BAO	TT+lowP+SN+BAO+ $H(z)$
$\Omega_b h^2$	0.02315 ± 0.00020	0.02305 ± 0.00020	0.02306 ± 0.00020
$\Omega_c h^2$	0.1097 ± 0.0011	0.1096 ± 0.0011	0.1097 ± 0.0010
$100\theta_{MC}$	1.04227 ± 0.00042	1.04219 ± 0.00041	1.04221 ± 0.00041
τ	0.131 ± 0.018	0.134 ± 0.017	0.133 ± 0.017
$\ln(10^{10} A_s)$	3.171 ± 0.036	3.178 ± 0.034	3.175 ± 0.034
Ω_k	-0.0122 ± 0.0044	-0.0079 ± 0.0021	-0.0074 ± 0.0020
w	-1.22 ± 0.19	-0.974 ± 0.0033	-0.968 ± 0.033
H_0 [km s $^{-1}$ Mpc $^{-1}$]	71.6 ± 4.7	67.26 ± 0.80	67.34 ± 0.74
Ω_m	0.264 ± 0.034	0.2949 ± 0.0072	0.2944 ± 0.0066
σ_8	0.888 ± 0.050	0.824 ± 0.017	0.822 ± 0.017
Parameter	TT+lowP+ $f\sigma_8$	TT+lowP+BAO+ $f\sigma_8$	TT+lowP+SN+BAO+ $H(z)$ + $f\sigma_8$
$\Omega_b h^2$	0.02311 ± 0.00020	0.02307 ± 0.00019	0.02307 ± 0.00020
$\Omega_c h^2$	0.1090 ± 0.0010	0.1092 ± 0.0011	0.1092 ± 0.0010
$100\theta_{MC}$	1.04226 ± 0.00041	1.04224 ± 0.00041	1.04224 ± 0.00042
τ	0.119 ± 0.019	0.126 ± 0.017	0.125 ± 0.016
$\ln(10^{10} A_s)$	3.146 ± 0.038	3.160 ± 0.034	3.159 ± 0.033
Ω_k	-0.0089 ± 0.0077	-0.0070 ± 0.0024	-0.0071 ± 0.0020
w	-1.22 ± 0.18	-0.951 ± 0.054	-0.961 ± 0.033
H_0 [km s $^{-1}$ Mpc $^{-1}$]	74.9 ± 8.1	67.1 ± 1.1	67.41 ± 0.77
Ω_m	0.245 ± 0.054	0.295 ± 0.010	0.2926 ± 0.0068
σ_8	0.880 ± 0.058	0.808 ± 0.018	0.811 ± 0.016

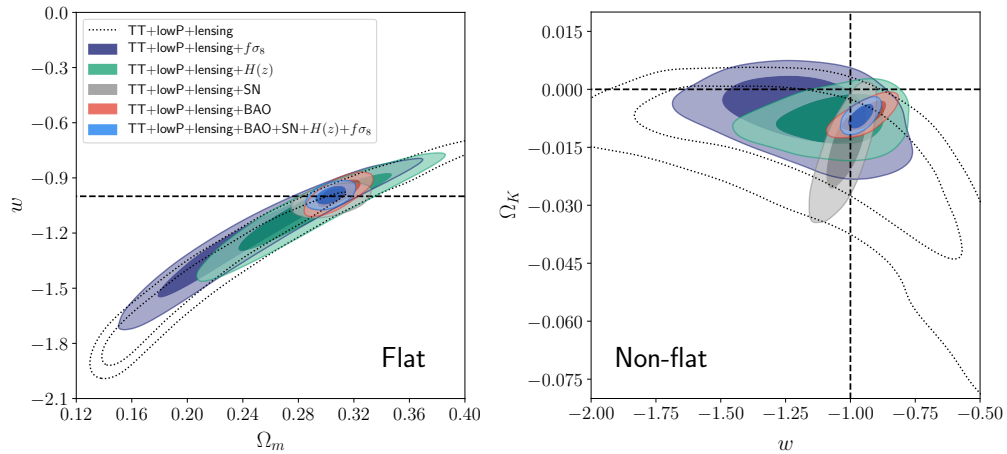


Figure 6. 1σ and 2σ likelihood contours in the Ω_m - w plane for the tilted flat- Λ CDM parameterization (left panel) and in the w - Ω_k plane for the untilted nonflat Λ CDM parameterization (right panel), constrained by Planck CMB TT + lowP + lensing and non-CMB data sets. The horizontal and vertical dashed lines indicate $w = -1$ (the cosmological constant) or $\Omega_k = 0$. Contours in both panels follow the color scheme shown in the left panel.

Table 6Untilted nonflat Λ CDM model parameters constrained with Planck TT + lowP + lensing, SN, BAO, $H(z)$, and $f\sigma_8$ data (mean and 68.3% confidence limits).

Parameter	TT+lowP+lensing	TT+lowP+lensing+SN	TT+lowP+lensing+BAO
$\Omega_b h^2$	0.02305 ± 0.00020	0.02305 ± 0.00019	0.02302 ± 0.00020
$\Omega_c h^2$	0.1091 ± 0.0011	0.1091 ± 0.0011	0.1094 ± 0.0011
$100\theta_{MC}$	1.04235 ± 0.00043	1.04234 ± 0.00041	1.04226 ± 0.00041
τ	0.100 ± 0.022	0.101 ± 0.021	0.123 ± 0.014
$\ln(10^{10} A_s)$	3.106 ± 0.044	3.109 ± 0.042	3.154 ± 0.027
Ω_k	-0.019 ± 0.017	-0.0153 ± 0.0075	-0.0070 ± 0.0025
w	-1.12 ± 0.39	-1.019 ± 0.053	-0.946 ± 0.056
H_0 [km s ⁻¹ Mpc ⁻¹]	69 ± 14	65.5 ± 2.3	66.9 ± 1.2
Ω_m	0.31 ± 0.13	0.310 ± 0.021	0.297 ± 0.010
σ_8	0.83 ± 0.11	0.803 ± 0.015	0.805 ± 0.014
Parameter	TT+lowP+lensing+ $H(z)$	TT+lowP+lensing+SN+BAO	TT+lowP+lensing+SN+BAO+ $H(z)$
$\Omega_b h^2$	0.02304 ± 0.00020	0.02303 ± 0.00019	0.02303 ± 0.00021
$\Omega_c h^2$	0.1094 ± 0.0011	0.1094 ± 0.0011	0.1095 ± 0.0010
$100\theta_{MC}$	1.04232 ± 0.00043	1.04228 ± 0.00040	1.04228 ± 0.00041
τ	0.114 ± 0.017	0.120 ± 0.012	0.121 ± 0.012
$\ln(10^{10} A_s)$	3.137 ± 0.034	3.148 ± 0.024	3.150 ± 0.024
Ω_k	-0.0081 ± 0.0042	-0.0075 ± 0.0021	-0.0070 ± 0.0020
w	-1.06 ± 0.14	-0.967 ± 0.033	-0.961 ± 0.033
H_0 [km s ⁻¹ Mpc ⁻¹]	69.9 ± 4.2	67.31 ± 0.77	67.38 ± 0.75
Ω_m	0.275 ± 0.033	0.2938 ± 0.0069	0.2933 ± 0.0067
σ_8	0.832 ± 0.036	0.809 ± 0.011	0.809 ± 0.011
Parameter	TT+lowP+lensing+ $f\sigma_8$	TT+lowP+lensing+BAO+ $f\sigma_8$	TT+lowP+lensing+SN+BAO+ $H(z)$ + $f\sigma_8$
$\Omega_b h^2$	0.02306 ± 0.00020	0.02303 ± 0.00020	0.02305 ± 0.00020
$\Omega_c h^2$	0.1090 ± 0.0011	0.1093 ± 0.0011	0.1092 ± 0.0010
$100\theta_{MC}$	1.04229 ± 0.00041	1.04225 ± 0.00043	1.04227 ± 0.00042
τ	0.114 ± 0.019	0.120 ± 0.013	0.119 ± 0.012
$\ln(10^{10} A_s)$	3.136 ± 0.038	3.148 ± 0.026	3.146 ± 0.024
Ω_k	-0.0056 ± 0.0063	-0.0068 ± 0.0024	-0.0069 ± 0.0020
w	-1.19 ± 0.18	-0.943 ± 0.054	-0.960 ± 0.032
H_0 [km s ⁻¹ Mpc ⁻¹]	76.4 ± 8.3	67.0 ± 1.1	67.45 ± 0.75
Ω_m	0.236 ± 0.053	0.297 ± 0.010	0.2923 ± 0.0066
σ_8	0.873 ± 0.059	0.801 ± 0.014	0.805 ± 0.011

power (Figs. 9b).

5. CONCLUSION

We measure cosmological parameters from an updated, reliable, large compilation of observational data by using the tilted flat- Λ CDM and the untilted nonflat Λ CDM dynamical dark energy inflation parameterizations.

In summary, our main results are:

- We confirm, but at lower significance, the Ooba et al. (2018d) result that the tilted flat- Λ CDM parameterization provides a better fit to the data than does the standard tilted flat- Λ CDM model. The improvement is not significant, but on the other hand current data are unable to rule out dynamical dark energy.
- In the untilted nonflat Λ CDM case, we confirm, at higher significance, the Ooba et al. (2018b) result that cosmological data does not demand spatially-flat hypersurfaces for this parameterization, and that the nonflat Λ CDM parameterization provides a better fit to the data than does the nonflat Λ CDM model (qualitatively it is clear that the standard tilted flat- Λ CDM model is a better fit to the data than is the untilted nonflat Λ CDM model). In the nonflat Λ CDM case, these data (including CMB lensing measurements) favor a closed model at more than 3.4σ significance, with spatial curvature contributing a little less than a percent to the current cosmological energy budget, and favor dark energy dynamics (over a cosmological constant) at a little more than 1.2σ .
- H_0 values measured in both models are very similar, and consistent with many other measurements of H_0 . However, as well known, H_0 estimated from the local expansion rate (Riess et al. 2018) is about 3σ larger.
- σ_8 values measured in both models are close to identical and compatible with the recent DES measurement (DES Collaboration 2018).
- The measured Ω_m value is more model dependent than the measured σ_8 value and the Ω_m value measured using the nonflat Λ CDM parameterization is more consistent with the recent DES estimate (DES Collaboration 2018).
- $\Omega_b h^2$, τ , $\Omega_c h^2$, as well as some of the other measured cosmological parameter values are model dependent.

We thank D. Scolnic for providing us the Pantheon data. We acknowledge valuable discussions with C. Bennett, J. Ooba, and D. Scolnic. C.-G.P. was supported by the Basic Science Research Program through the National Research Foundation of Korea (NRF) funded by the Ministry of Education (No. 2017R1D1A1B03028384). B.R. was supported in part by DOE grant DE-SC0019038.

REFERENCES

- Addison, G. E., Huang, Y., Watts, D. J., et al. 2016, *ApJ*, 818, 132 [arXiv:1511.00055]
 Alam, S., Ata, M., Bailey, S., et al. 2017, *MNRAS*, 470, 2617 [arXiv:1607.03155]
 Ata, M., Baumgarten, F., Bautista, J., et al. 2018, *MNRAS*, 473, 4773 [arXiv:1705.06373]
 Aubourg, É., Bailey, S., Bautista, J. E., et al. 2015, *Phys. Rev. D*, 92, 123516 [arXiv:1411.1074]
 Audren, B., Lesgourgues, J., Benabed, K., & Prunet, S. 2013, *JCAP*, 1302, 001 [arXiv:1210.7183]
 Aylor, K., Hou, Z., Knox, L., et al. 2017, *ApJ*, 850, 101 [arXiv:1706.10286]
 Betoule, M., Kessler, R., Guy, J., et al. 2014, *A&A*, 568, A22 [arXiv:1401.4064]
 Blas, D., Lesgourgues, J., & Tram, T. 2011, *JCAP*, 1107, 034 [arXiv:1104.2933]
 Brax, P. 2018, *Rep. Prog. Phys.*, 81, 016902
 Cai, R.-G., Guo, Z.-K., & Yang, T. 2016, *Phys. Rev. D*, 93, 043517 [arXiv:1509.06283]
 Cao, S.-L., Duan, X.-W., Meng, X.-L., & Zhang, T.-J. 2018, *Eur. Phys. J.*, C78, 313 [arXiv:1712.01703]
 Challinor, A., & Lasenby, A. 1999, *ApJ*, 513, 1 [arXiv:astro-ph/9804301]
 Chen, G., Gott, J. R., & Ratra, B. 2003, *PASP*, 115, 1269 [arXiv:astro-ph/0308099]
 Chen, G., & Ratra, B. 2004, *ApJ*, 612, L1 [arXiv:astro-ph/0405636]
 Chen, G., & Ratra, B. 2011a, *PASP*, 123, 1127 [arXiv:1105.5206]
 Chen, Y., Kumar, S., & Ratra, B. 2017, *ApJ*, 835, 86 [arXiv:1606.07316]
 Chen, Y., & Ratra, B. 2011b, *Phys. Lett. B*, 703, 406 [arXiv:1106.4294]
 Chen, Y., Ratra, B., Biesiada, M., Li, S., & Zhu, Z.-H. 2016, *ApJ*, 829, 61 [arXiv:1603.07115]
 DES Collaboration, Abbott, T. M. C., Abdalla, F. B., Alarcon, A., et al. 2018, *Phys. Rev. D*, 98, 043526 [arXiv:1708.01530]
 DES Collaboration, Abbott, T. M. C., Abdalla, F. B., Annis, J., et al. 2017, arXiv:1711.00403
 Dhawan, S., Jha, S. W., & Leibundgut, B. 2018, *A&A*, 609, A72 [arXiv:1707.00715]
 Ding, X., Biesiada, M., Cao, S., Li, Z., & Zhu, Z.-H. 2015, *ApJ*, 803, L22 [arXiv:1503.04923]
 Farooq, O., Madiyar, F. R., Crandall, S., & Ratra, B. 2017, *ApJ*, 835, 26 [arXiv:1607.03537]
 Farooq, O., Mania, D., & Ratra, B. 2015, *ApSS*, 357, 11 [arXiv:1308.0834]
 Farooq, O., & Ratra, B. 2013, *ApJ*, 766, L7 [arXiv:1301.5243]
 Fernández Arenas, D., Terlevich, E., Terlevich, R., et al. 2018, *MNRAS*, 474, 1250 [arXiv:1710.05951]
 Gómez-Valent, A., & Amendola, L. 2018, *JCAP*, 1804, 031 [arXiv:1802.01505]
 Gómez-Valent, A., & Solà, J. 2017, *Europhys. Lett.*, 120, 39001 [arXiv:1711.00692]
 Gómez-Valent, A., & Solà, J. 2018, arXiv:1801.08501
 Gott, J. R. 1982, *Nature*, 295, 304
 Gott, J. R., Vogeley, M. S., Podariu, S., & Ratra, B. 2001, *ApJ*, 549, 1 [arXiv:astro-ph/0006103]
 Haridasu, B. S., Luković, V. V., & Vittorio, N. 2018, *JCAP*, 1805, 033 [arXiv:1711.03929]
 Hawking, S. W. 1984, *Nucl. Phys. B*, 239, 257
 Lewis, A., & Bridle, S. 2002, *Phys. Rev. D*, 66, 103511 [arXiv:astro-ph/0205436]
 Lewis, A., Challinor, A., & Lasenby, A. 2000, *ApJ*, 538, 473 [arXiv:astro-ph/9911177]
 L’Huillier, B., & Shafieloo, A. 2017, *JCAP*, 1701, 015 [arXiv:1606.06832]
 Li, Z., Wang, G.-J., Liao, K., & Zhu, Z.-H. 2016, *ApJ*, 833, 240 [arXiv:1611.00359]
 Lin, W., & Ishak, M. 2017, *Phys. Rev. D*, 96, 083532 [arXiv:1708.09813]
 Lucchin, F., & Matarrese, S. 1985, *Phys. Rev. D*, 32, 1316
 Luković, V. V., D’Agostino, R., & Vittorio, N. 2016, *A&A*, 595, A109 [arXiv:1607.05677]
 Luković, V. V., Haridasu, B. S., & Vittorio, N. 2018, arXiv:1801.05765
 Martin, J. 2012, *C. R. Physique*, 13, 566 [arXiv:1205.3365]
 Mitra, S., Choudhury, T. R., & Ratra, B. 2018, *MNRAS*, 479, 4566 [arXiv:1712.00018]
 Mitra, S., Park, C.-G., Choudhury, T. R., & Ratra, B. 2019, arXiv:1901.09927
 Moresco, M., Pozzetti, L., Cimatti, A., et al. 2016, *JCAP*, 1605, 014 [arXiv:1601.01701]
 Ooba, J., Ratra, B., & Sugiyama, N. 2018a, *ApJ*, 864, 80 [arXiv:1707.03452]
 Ooba, J., Ratra, B., & Sugiyama, N. 2018b, *ApJ*, 869, 34 [arXiv:1710.03271]
 Ooba, J., Ratra, B., & Sugiyama, N. 2018c, *ApJ*, 866, 68 [arXiv:1712.08617]
 Ooba, J., Ratra, B., & Sugiyama, N. 2018d, arXiv:1802.05571
 Park, C.-G., & Ratra, B. 2018a, arXiv:1801.00213
 Park, C.-G., & Ratra, B. 2018b, *ApJ*, 868, 83 [arXiv:1807.07421]
 Park, C.-G., & Ratra, B. 2018c, arXiv:1809.03598
 Pavlov, A., Westmoreland, S., Saaidi, K., & Ratra, B. 2013, *Phys. Rev. D*, 88, 123513 [arXiv:1307.7399]
 Peebles, P. J. E. 1984, *ApJ*, 284, 439
 Peebles, P. J. E., & Ratra, B. 1988, *ApJ*, 325, L17
 Penton, J., Peyton, J., Zahoor, A., & Ratra, B. 2018, *PASP*, 130, 114009 [arXiv:1808.01490]
 Planck Collaboration 2015, *Planck 2015 Results: Cosmological Parameter Tables at wiki.cosmos.esa.int/planckpla2015/images/f/f7/Baseline_parameters_table_2015_limit68.pdf*

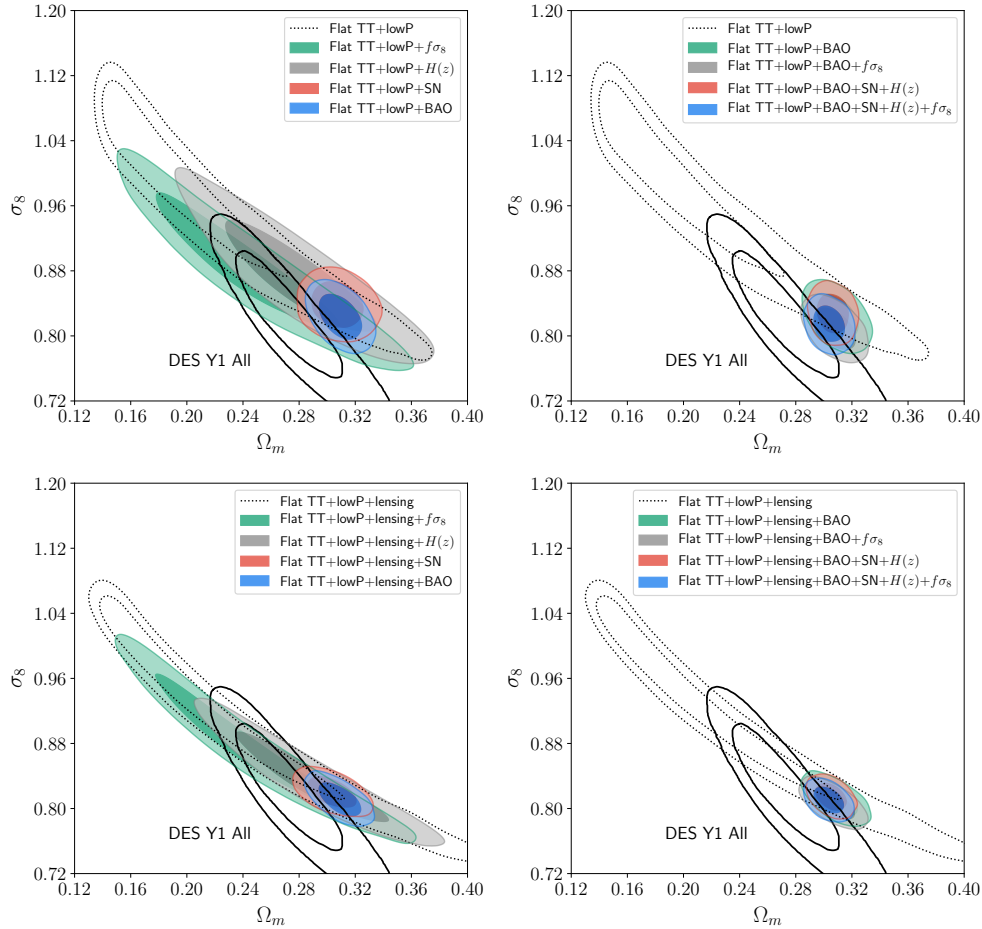


Figure 7. 1σ and 2σ likelihood contours in the Ω_m - σ_8 plane for the tilted flat-XCDM parameterization constrained by Planck CMB TT + lowP (+lensing), SNIa, BAO, $H(z)$, and $f\sigma_8$ data. In each panel the Λ CDM model 1σ and 2σ constraint contours obtained from the first-year Dark Energy Survey (DES Y1 All) (DES Collaboration 2018) are shown as thick solid curves for comparison.

Planck Collaboration, Ade, P. A. R., Aghanim, N., Arnaud, M., et al. 2016, *A&A*, 594, A13 [arXiv:1502.01589]
 Planck Collaboration, Aghanim, N., Akrami, Y., Ashdown, M., et al. 2017, *A&A*, 607, A95 [arXiv:1608.02487]
 Podariu, S., & Ratra, B. 2001, *ApJ*, 532, 109 [arXiv:astro-ph/9910527]
 Rana, A., Jain, D., Mahajan, S., & Mukherjee, A. 2017, *JCAP*, 1703, 028 [arXiv:1611.07196]
 Ratra, B. 1985, *Phys. Rev. D*, 31, 1931
 Ratra, B. 1989, *Phys. Rev. D*, 40, 3939
 Ratra, B. 1992, *Phys. Rev. D*, 45, 1913
 Ratra, B. 2017, *Phys. Rev. D*, 96, 103534 [arXiv:1707.03439]
 Ratra, B., & Peebles, P. J. E. 1988, *Phys. Rev. D*, 37, 3406
 Ratra, B., & Peebles, P. J. E. 1994, *ApJ*, 432, L5
 Ratra, B., & Peebles, P. J. E. 1995, *Phys. Rev. D*, 52, 1837
 Ratra, B., & Vogeley, M. 2008, *PASP*, 120, 235 [arXiv:0706.1565]
 Riess, A. G., Casertano, S., Yuan, E., et al. 2018, *ApJ*, 855, 136 [arXiv:1801.01120]
 Rigault, M., Aldering, G., Kowalski, M., et al. 2015, *ApJ*, 802, 20 [arXiv:1412.6501]
 Ryan, J., Chen, Y., & Ratra, B. 2019, arXiv:1902.03196
 Ryan, J., Doshi, S., & Ratra, B. 2018, *MNRAS*, 480, 759 [arXiv:1805.06408]
 Sahni, V., Shafieloo, A., & Starobinsky, A. A. 2014, *ApJ*, 793, L4 [arXiv:1406.2209]
 Samushia, L., Chen, G., & Ratra, B. 2007, arXiv:0706.1963
 Samushia, L., & Ratra, B. 2010, *ApJ*, 714, 1347 [arXiv:0905.3836]
 Scolnic, D. M., Jones, D. O., Rest, A., et al. 2017, arXiv:1710.00845
 Semiz, I., & Çamlıbel, A. K. 2015, *JCAP*, 1512, 038 [arXiv:1505.04043]
 Solà, J., de Cruz Pérez, J., & Gómez-Valent, A. 2018, *Europhys. Lett.*, 121, 39001 [arXiv:1606.00450]

Solà, J., de Cruz Pérez, J., & Gómez-Valent, A. 2017c, arXiv:1703.08218
 Solà, J., Gómez-Valent, A., & de Cruz Pérez, J. 2015, *ApJ*, 811, L14 [arXiv:1506.05793]
 Solà, J., Gómez-Valent, A., & de Cruz Pérez, J. 2017a, *ApJ*, 836, 43 [arXiv:1602.02103]
 Solà, J., Gómez-Valent, A., & de Cruz Pérez, J. 2017b, *Mod. Phys. Lett. A*, 32, 1750054 [arXiv:1610.08965]
 Solà, J., Gómez-Valent, A., & de Cruz Pérez, J. 2017d, *Phys. Lett. B*, 774, 317 [arXiv:1705.06723]
 Wang, F. Y., Dai, Z. G., & Shi, Q. 2009, *A&A*, 507, 53 [arXiv:0912.5141]
 Wang, F. Y., Dai, Z. G., & Zhu, Z.-H. 2007, *ApJ*, 667, 1 [arXiv:0706.0938]
 Wang, Y., Xu, L., & Zhao, G.-B. 2017, *ApJ*, 849, 84 [arXiv:1706.09149]
 Wei, J.-J., & Wu, X.-F. 2017, *ApJ*, 838, 160 [arXiv:1611.00904]
 Yu, H., Ratra, B., & Wang, F.-Y. 2018, *ApJ*, 856, 3 [arXiv:1711.03437]
 Yu, H., & Wang, F. Y. 2016, *ApJ*, 828, 85 [arXiv:1605.02483]
 Zhai, Z., Blanton, M., Slosar, A., & Tinker, J. 2017, *ApJ*, 850, 183 [arXiv:1705.10031]
 Zhang, B. R., Childress, M. J., Davis, T. M., et al. 2017b, *MNRAS*, 471, 2254 [arXiv:1706.07573]
 Zhang, X., Huang, Q.-G., & Li, X.-D. 2018, arXiv:1801.07403
 Zhang, Y.-C., Zhang, H.-Y., Wang, D.-D., et al. 2017a, *Res. Astron. Astrophys.*, 17, 6 [arXiv:1703.08293]
 Zhao, G.-B., Raveri, M., Pogosian, L., et al. 2017, *Nat. Astron.*, 1, 627 [arXiv:1701.08165]
 Zhao, G.-B., Xia, J. Q., Li, H., et al. 2007, *Phys. Lett. B*, 648, 8 [arXiv:astro-ph/0612788]
 Zheng, X., Ding, X., Biesiada, M., Cao, S., & Zhu, Z.-H. 2016, *ApJ*, 825, 17 [arXiv:1604.07910]

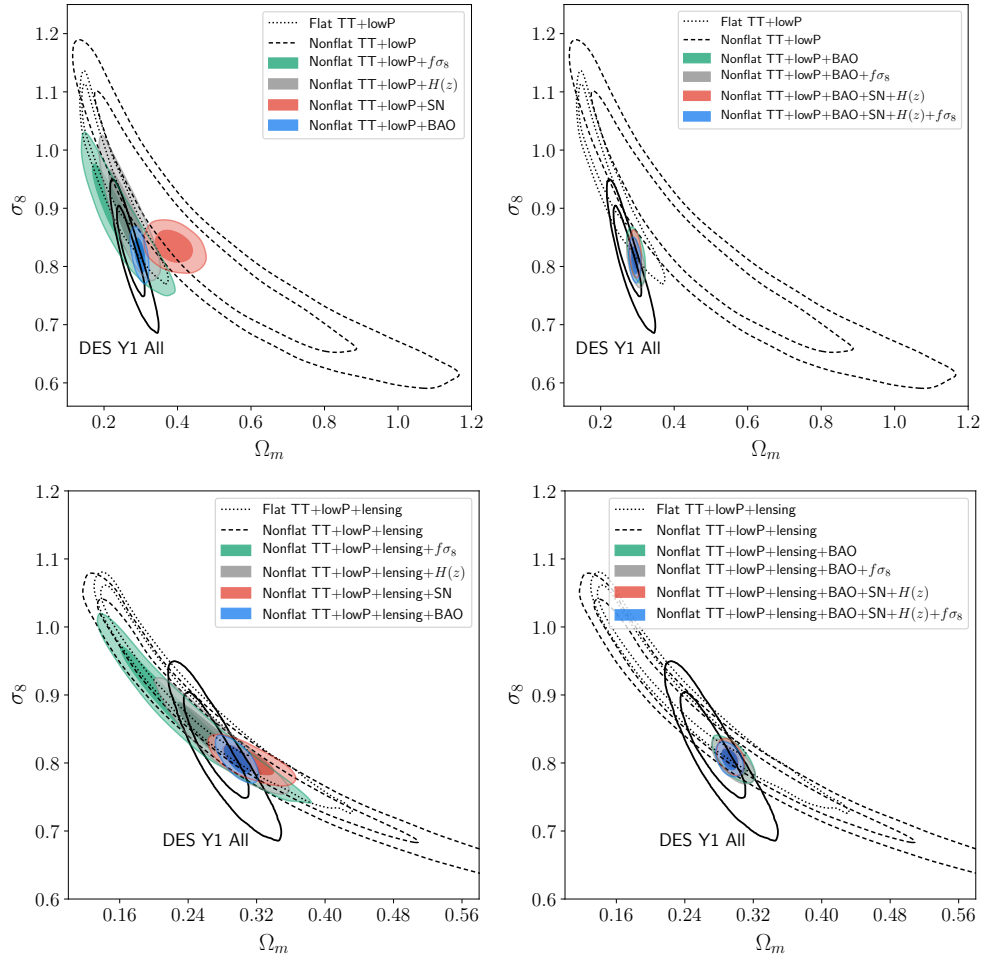


Figure 8. Same as Fig. 7 but for the untitled nonflat XCDM parameterization.

Table 7
Individual and total χ^2 values for the best-fit tilted flat and untilted nonflat Λ CDM inflation models.

Data sets	χ^2_{PHKTT}	χ^2_{lowTEB}	χ^2_{lensing}	χ^2_{SN}	χ^2_{BAO}	$\chi^2_{H(z)}$	$\chi^2_{f\sigma_8}$	χ^2_{prior}	Total χ^2	$\Delta\chi^2$
Tilted flat- Λ CDM model										
TT+lowP	763.57	10496.41						1.96	11261.93	
+SN	763.45	10496.50		1036.29				2.06	12298.31	
+BAO	764.20	10495.92			13.02			2.12	11275.25	
+ $H(z)$	763.98	10496.36				14.89		1.70	11276.93	
+ $f\sigma_8$	766.83	10494.95					12.15	1.87	11275.80	
+BAO+ $f\sigma_8$	766.67	10494.83			12.64		12.40	1.96	11288.50	
+SN+BAO	764.34	10495.96		1036.15	12.93			2.03	12311.41	
+SN+BAO+ $H(z)$	764.33	10495.93		1036.15	12.95	14.83		2.03	12326.21	
+SN+BAO+ $H(z)$ + $f\sigma_8$	766.68	10494.90		1036.02	12.71	14.79	12.38	1.88	12339.36	
TT+lowP+lensing	766.20	10494.93	9.30					2.00	11272.44	
+SN	766.53	10494.83	9.17	1036.05				2.02	12308.59	
+BAO	766.44	10494.80	9.13		12.61			2.09	11285.07	
+ $H(z)$	766.20	10494.92	9.27			14.83		2.04	11287.27	
+ $f\sigma_8$	768.26	10494.43	8.67				11.31	1.94	11284.62	
+BAO+ $f\sigma_8$	767.56	10494.49	8.71		12.59		11.80	2.16	11297.32	
+SN+BAO	766.53	10494.77	9.03	1036.07	12.61			2.16	12321.17	
+SN+BAO+ $H(z)$	766.51	10494.80	9.07	1036.07	12.61	14.81		2.14	12336.01	
+SN+BAO+ $H(z)$ + $f\sigma_8$	767.61	10494.48	8.74	1036.01	12.68	14.79	11.84	2.04	12348.20	
Untilted nonflat Λ CDM model										
TT+lowP	774.34	10495.42						2.33	11272.10	10.17
+SN	778.23	10497.99		1036.74				1.97	12314.94	16.63
+BAO	780.27	10499.20			14.69			1.92	11296.08	20.83
+ $H(z)$	777.14	10500.93				17.11		1.96	11297.15	20.22
+ $f\sigma_8$	783.38	10497.49					11.51	2.41	11294.79	18.99
+BAO+ $f\sigma_8$	783.46	10497.40			14.01		10.72	1.81	11307.41	18.91
+SN+BAO	780.65	10499.11		1036.11	14.56			1.86	12332.30	20.89
+SN+BAO+ $H(z)$	782.84	10497.40		1036.18	14.06	16.17		1.91	12348.57	22.36
+SN+BAO+ $H(z)$ + $f\sigma_8$	781.14	10499.17		1036.29	14.17	16.14	11.32	1.74	12359.98	20.62
TT+lowP+lensing	786.87	10493.86	9.77					1.79	11292.29	19.85
+SN	786.65	10494.69	9.19	1035.95				1.83	12328.31	19.72
+BAO	784.19	10497.32	9.86		13.99			2.04	11307.40	22.33
+ $H(z)$	786.87	10496.02	8.66			16.36		2.19	11310.10	22.83
+ $f\sigma_8$	786.41	10496.00	8.75				9.79	1.99	11302.93	18.31
+BAO+ $f\sigma_8$	788.21	10494.90	8.38		13.89		9.81	2.11	11317.31	19.99
+SN+BAO	784.76	10496.50	9.54	1036.23	13.87			1.89	12342.79	21.62
+SN+BAO+ $H(z)$	784.72	10496.49	9.60	1036.24	13.84	16.11		1.89	12358.87	22.86
+SN+BAO+ $H(z)$ + $f\sigma_8$	786.96	10495.37	8.63	1036.37	13.81	16.07	9.77	1.90	12368.86	20.66

Note: $\Delta\chi^2$ of an untilted nonflat Λ CDM model estimated for a combination of data sets represents the excess value relative to χ^2 of the tilted flat- Λ CDM model for the same combination of data sets.

Table 8
Individual and total χ^2 values for the best-fit tilted flat and untilted nonflat XCDM inflation parameterizations.

Data sets	χ^2_{PHKTT}	χ^2_{lowTEB}	χ^2_{lensing}	χ^2_{SN}	χ^2_{BAO}	$\chi^2_{H(z)}$	$\chi^2_{f\sigma_8}$	χ^2_{prior}	Total χ^2	$\Delta\chi^2$
Tilted flat-XCDM parameterization										
TT+lowP	761.85	10495.08						2.02	11258.94	-2.99
+SN	763.24	10496.38		1035.93				2.10	12297.64	-0.67
+BAO	764.30	10496.20			12.76			1.94	11275.20	-0.05
+H(z)	763.32	10496.10				15.00		1.76	11276.18	-0.75
+f σ_8	766.16	10494.26					11.77	2.03	11274.21	-1.59
+BAO+f σ_8	766.79	10495.00			12.11		12.20	2.14	11288.24	-0.26
+SN+BAO	764.46	10495.90		1036.02	13.15			1.88	12311.39	-0.02
+SN+BAO+H(z)	764.33	10496.04		1036.09	13.16	14.82		1.80	12326.24	+0.03
+SN+BAO+H(z)+f σ_8	766.81	10494.83		1036.06	12.60	14.79	12.12	2.09	12339.31	-0.05
TT+lowP+lensing	766.09	10493.81	9.39					2.02	11271.31	-1.13
+SN	766.35	10494.78	9.24	1035.95				2.01	12308.33	-0.26
+BAO	767.00	10494.74	9.06		12.25			1.94	11284.99	-0.08
+H(z)	765.98	10494.66	9.37			14.89		2.21	11287.10	-0.17
+f σ_8	767.98	10493.86	8.65				10.77	1.92	11283.18	-1.44
+BAO+f σ_8	768.00	10494.68	8.69		11.98		11.60	2.01	11296.96	-0.36
+SN+BAO	766.61	10494.75	9.04	1036.10	12.58			2.09	12321.17	+0.00
+SN+BAO+H(z)	766.79	10494.76	9.06	1036.06	12.65	14.80		1.97	12336.08	+0.07
+SN+BAO+H(z)+f σ_8	767.76	10494.51	8.72	1036.06	12.54	14.80	11.76	1.97	12348.12	-0.08
Untilted nonflat XCDM parameterization										
TT+lowP	771.27	10499.28						2.55	11273.11	+1.01
+SN	773.06	10496.25		1036.87				1.97	12308.14	-6.80
+BAO	780.39	10500.33			12.71			2.10	11295.53	-0.55
+H(z)	774.60	10499.77				19.31		1.97	11295.64	-1.51
+f σ_8	779.82	10498.34					11.85	1.75	11291.75	-3.04
+BAO+f σ_8	780.68	10500.54			12.36		11.41	1.83	11306.82	-0.59
+SN+BAO	777.67	10504.10		1036.15	12.73			2.03	12332.68	+0.38
+SN+BAO+H(z)	778.12	10502.60		1036.03	13.24	16.00		1.88	12347.88	-0.69
+SN+BAO+H(z)+f σ_8	782.42	10499.28		1036.33	12.20	15.57	10.77	1.94	12358.52	-1.46
TT+lowP+lensing	785.83	10495.22	9.99					2.39	11293.44	+1.15
+SN	786.69	10494.26	9.79	1035.91				1.97	12328.62	+0.31
+BAO	784.55	10498.30	9.15		11.66			1.84	11305.50	-1.90
+H(z)	785.33	10497.40	8.83			15.58		2.00	11309.15	-0.95
+f σ_8	786.23	10497.02	8.69				8.40	2.23	11302.58	-0.35
+BAO+f σ_8	785.97	10497.57	8.63		11.73		9.81	1.70	11315.41	-1.90
+SN+BAO	785.67	10497.62	8.87	1036.15	12.37			2.30	12342.98	+0.19
+SN+BAO+H(z)	784.07	10498.25	9.33	1036.75	11.88	15.43		2.40	12358.11	-0.76
+SN+BAO+H(z)+f σ_8	784.99	10498.46	8.94	1036.51	12.09	15.56	9.83	1.72	12368.10	-0.76

Note: $\Delta\chi^2$ of tilted flat or untilted nonflat XCDM parameterization estimated for a combination of data sets represents the excess value relative to χ^2 of the corresponding Λ CDM model for the same combination of data sets.

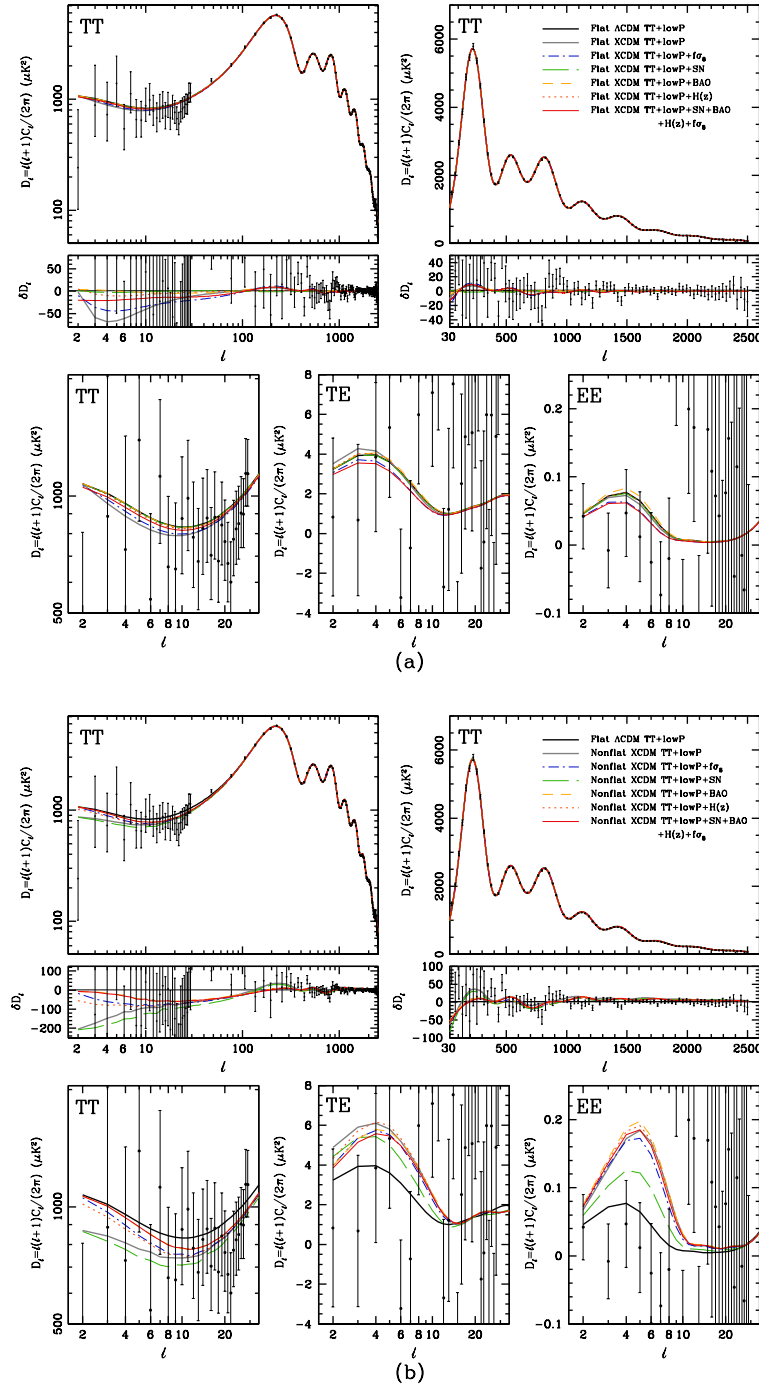


Figure 9. Best-fit CMB anisotropy power spectra of (a) tilted flat (top five panels) and (b) untilted nonflat XCDM parameterizations (bottom five panels) constrained by the Planck CMB TT + lowP data (excluding the lensing data) together with SN, BAO, $H(z)$, and $f\sigma_8$ data. For comparison, the best-fit power spectra of the tilted flat- Λ CDM model are shown as black curves. The residual δD_ℓ of the TT power spectra are shown with respect to the flat- Λ CDM power spectrum that best fits the TT + lowP data.

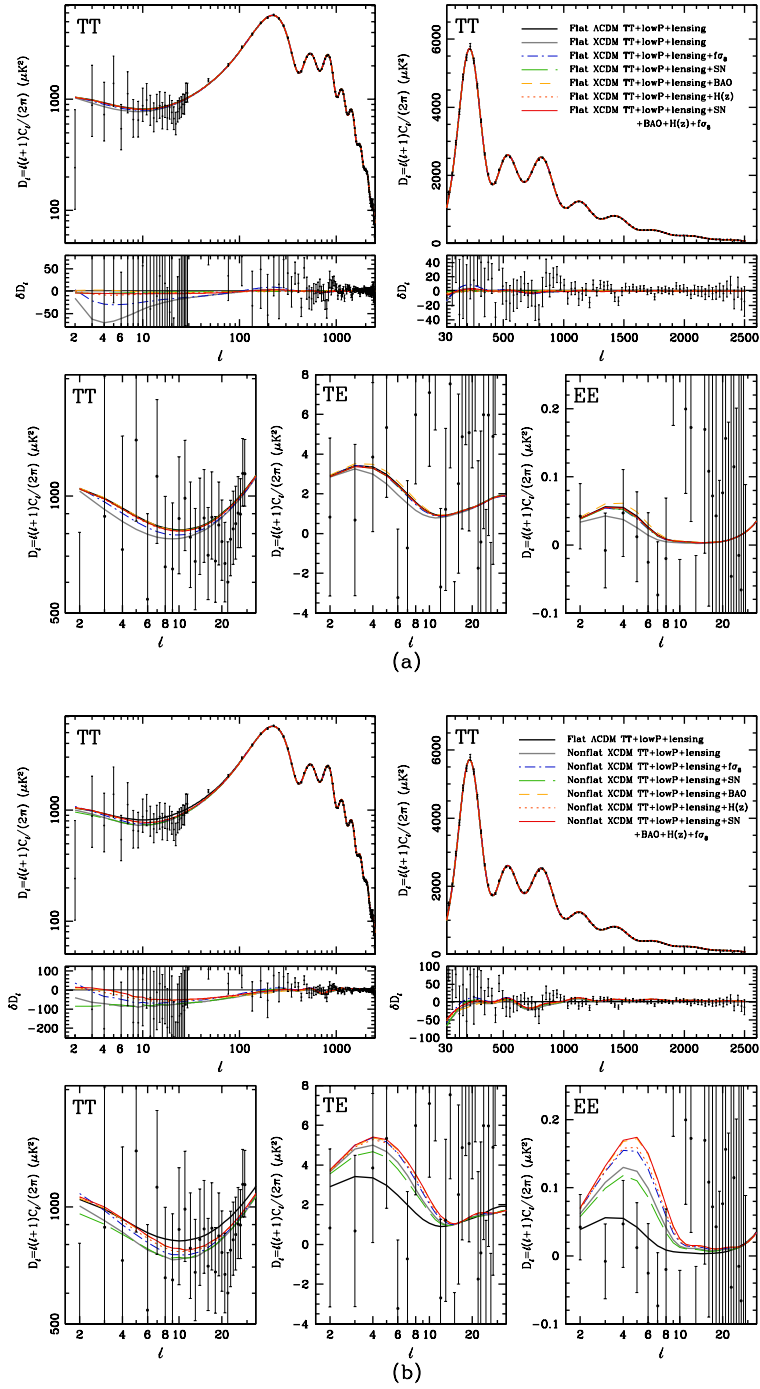


Figure 10. Same as Fig. 9 but now including the CMB lensing data. The residual δD_ℓ of the TT power spectra are shown with respect to the flat- Λ CDM power spectrum that best fits the TT + lowP + lensing data.

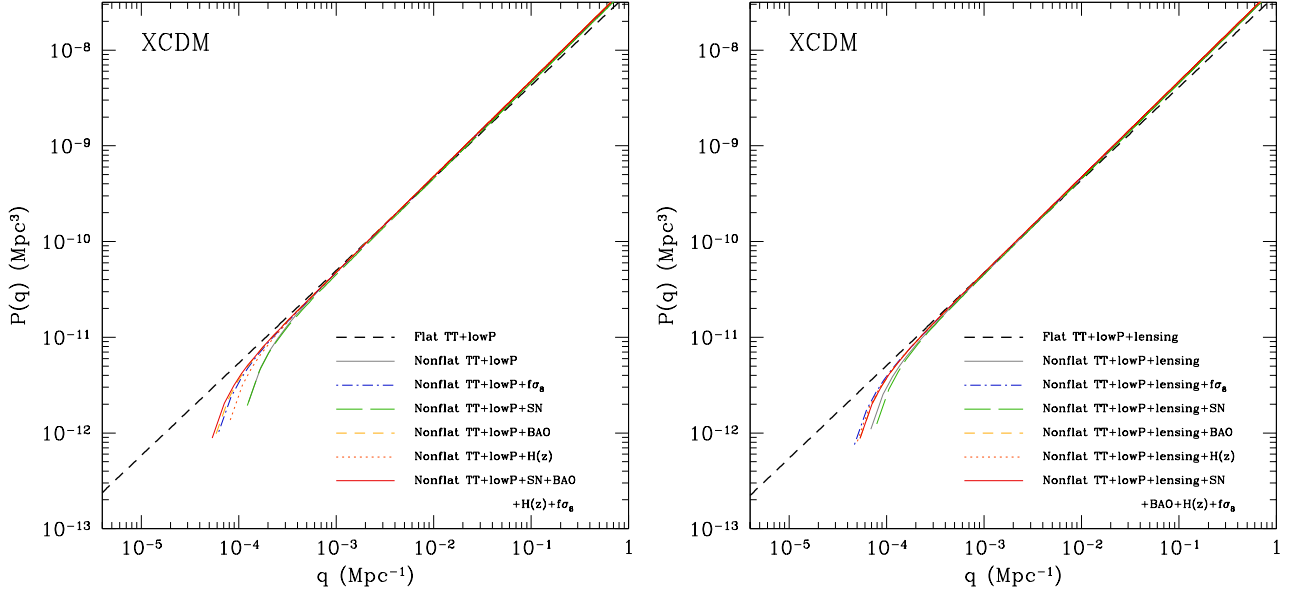


Figure 11. Power spectra of primordial scalar-type perturbations of best-fit untilted non-power-law power spectrum nonflat XCDM cases constrained using Planck TT + lowP data (left panel) and TT + lowP + lensing data (right panel) together with non-CMB data sets ($f\sigma_8$, SN, BAO, $H(z)$). In both panels the primordial power spectrum of the best-fit tilted flat-XCDM model is shown as dashed lines. For the definition of wavenumber q , see Sec. 3. The power spectrum is normalized to $P(q) = A_s$ at the pivot scale $k_0 = 0.05 \text{ Mpc}^{-1}$.